VOLUME 21 NUMBER 8 AUGUST 2009

THE PLANT CELL

MATE Transporters Facilitate Vacuolar Uptake of Epicatechin 3′-*O*-Glucoside for Proanthocyanidin Biosynthesis in *Medicago truncatula* and *Arabidopsis* [C][W]

Jian Zhao and Richard A. Dixon[1]

The Plant Cell, Vol. 21: 2323–2340, August 2009, www.plantcell.org © 2009 American Society of Plant Biologists

MATE Transporters Facilitate Vacuolar Uptake of Epicatechin 3′-*O*-Glucoside for Proanthocyanidin Biosynthesis in *Medicago truncatula* and *Arabidopsis* [C][W]

Jian Zhao and Richard A. Dixon[1]

Plant Biology Division, Samuel Roberts Noble Foundation, Ardmore, Oklahoma 73401

Expression of the *Arabidopsis thaliana* MYB transcription factor TRANSPARENT TESTA 2 (TT2) in *Medicago trunculata* hairy roots induces both proanthocyanidin accumulation and the ATP-dependent vacuolar/vesicular uptake of epicatechin 3′-*O*-glucoside; neither process is active in control roots that do, however, possess anthocyanidin 3-*O*-glucoside vacuolar uptake activity. A vacuolar membrane-localized multidrug and toxic compound extrusion (MATE) transporter, *Medicago* MATE1, was identified at the molecular level and shown to preferentially transport epicatechin 3′-*O*-glucoside. Genetic evidence has implicated TT12, a tonoplastic MATE transporter from *Arabidopsis*, in the transport of precursors for proanthocyanidin biosynthesis in the seed coat. However, although *Arabidopsis* TT12 facilitates the transport of cyanidin 3-*O*-glucoside into membrane vesicles when expressed in yeast, there is no evidence that cyanidin 3-*O*-glucoside is converted to proanthocyanidins after transport into the vacuole. Here, we show that *Arabidopsis* TT12, like *Medicago* MATE1, functions to transport epicatechin 3′-*O*-glucoside as a precursor for proanthocyanidin biosynthesis, and *Medicago* MATE1 complements the seed proanthocyanidin phenotype of the *Arabidopsis tt12* mutant both quantitatively and qualitatively. On the basis of biochemical properties, tissue-specific expression pattern, and genetic loss-of-function analysis, we conclude that MATE1 is an essential membrane transporter for proanthocyanidin biosynthesis in the *Medicago* seed coat. Implications of these findings for the assembly of oligomeric proanthocyanidins are discussed.

INTRODUCTION

Proanthocyanidins (PAs; also called condensed tannins) are oligomers of flavan-3-ol units and are found as prominent compounds in seed coats, leaves, fruits, flowers, and bark of many plant species (Ariga et al., 1981; Gabetta et al., 2000; Gu et al., 2004; Dixon et al., 2005). They are derived from the flavonoid/anthocyanin branch of the phenylpropanoid pathway. PAs and their presumed monomeric building blocks, such as catechin and epicatechin, are potent antioxidants with beneficial effects on cardiac health, immunity, and longevity (Santos-Buelga and Scalbert, 2000; Serafini et al., 2003). The presence of PAs in forage plants is regarded as a positive trait that protects ruminant animals from pasture bloat and enhances ruminant nutrition (Lees, 1992). It is therefore important to understand PA biosynthesis as a basis for metabolic engineering of PA production in plants.

In *Arabidopsis thaliana* and the model legume barrel medic (*Medicago truncatula*), the PAs found in the seed coat consist essentially of epicatechin units (Abrahams et al., 2002; Lepiniec et al., 2006; Pang et al., 2007) (Figure 1). Epicatechin and anthocyanins share a common biosynthetic pathway from Phe to anthocyanidin (Dixon et al., 2005), which is then converted to epicatechin by anthocyanidin reductase (ANR) (Xie et al., 2003). Characterization of a series of *Arabidopsis* mutants with pale-colored seeds (termed *transparent testa* [*tt*] or *tannin-deficient seeds* [*tds*]) has revealed many genes that are essential for PA and anthocyanin accumulation in seeds (Shirley et al., 1995; Abrahams et al., 2002; Lepiniec et al., 2006). The genes defined by the *tt* and *tds* mutations encode biosynthetic enzymes, such as ANR, regulatory transcription factors, and proteins involved in transport of intermediates in the PA and anthocyanin biosynthesis pathways (Lepiniec et al., 2006).

Anthocyanins and PAs accumulate in the vacuole, where polymerization of PA precursors is believed to occur followed by conversion to brown oxidation products (Lepiniec et al., 2006). However, the nature of the intermediates that are transported to the vacuole, and then polymerize to give PA oligomers, is not fully understood. ANR is a soluble cytoplasmic enzyme (Pang et al., 2007), and epicatechin or its derivatives destined for PA biosynthesis therefore likely have an extravacuolar origin. Blocking flavonoid transport from the cytosol into the central vacuole reduces anthocyanin and PA production, and ATP binding cassette (ABC) and multidrug and toxin extrusion (MATE) transporter proteins have been shown genetically to be involved in both anthocyanin and PA precursor transport (Debeaujon et al., 2001; Abrahams et al., 2003; Goodman et al., 2004). The *Arabidopsis TT12* gene was identified as encoding a MATE transporter that could transport potential PA precursor(s) into the vacuole (Debeaujon et al., 2001). Expression of *TT12* is

[1] Address correspondence to radixon@noble.org.
The author responsible for distribution of materials integral to the findings presented in this article in accordance with the policy described in the Instructions for Authors (www.plantcell.org) is: Richard A. Dixon (radixon@noble.org).
[C]Some figures in this article are displayed in color online but in black and white in the print edition.
[W]Online version contains Web-only data.
www.plantcell.org/cgi/doi/10.1105/tpc.109.067819

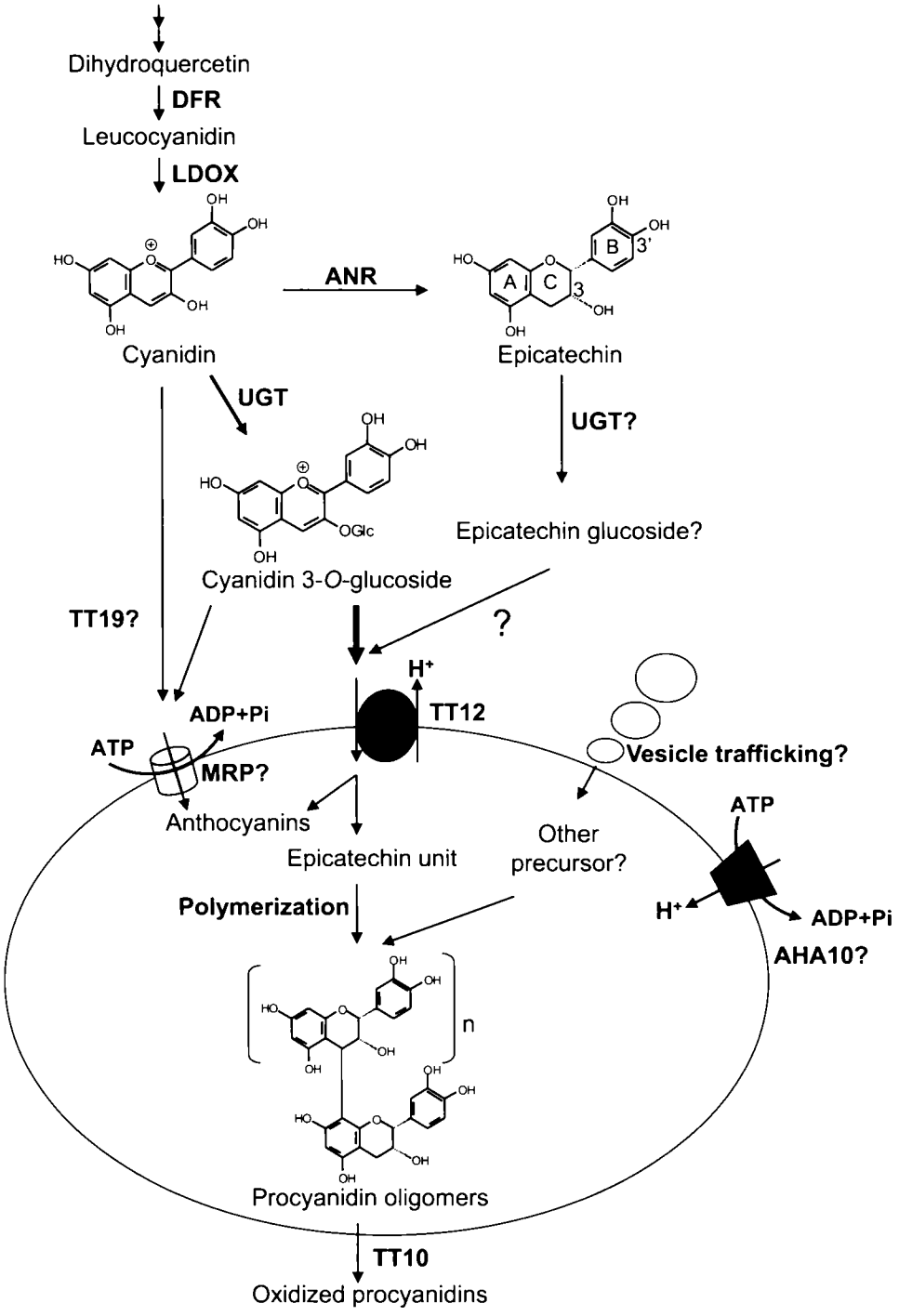

Figure 1. Diagrammatic Representation of Key Reactions for PA Precursor Synthesis and Transport in *Arabidopsis*.

Enzymes are as follows: DFR, dihydroflavonol reductase; LDOX, leucoanthocyanidin dioxygenase; UGT, uridine diphosphate glycosyltransferase; MRP, multidrug resistance-associated protein. [See online article for color version of this figure.]

regulated by the transcription factors TT2, TTG1, and TT8 in the *Arabidopsis* seed coat (Lepiniec et al., 2006). Membrane vesicles from yeast expressing *Arabidopsis* TT12 could transport cyanidin 3-*O* glucoside (Cy3G) (Figure 1) but not catechin 3-*O*-glucoside (C3G), and C3G strongly inhibited TT12-mediated Cy3G uptake (Marinova et al., 2007). This result, however, does not confirm the nature of the transported species or explain why the *tt12* mutant has reduced PA accumulation, since catechin is not a component of *Arabidopsis* seed coat PAs. In this regard, Marinova et al. (2007) suggested that TT12 might transport a

glucoside of epicatechin, but the exact nature of this compound was not described.

We have recently identified a *Medicago* uridine diphosphate glucosyltransferase, UGT72L1, with high specificity for production of epicatechin 3′-*O*-glucoside (E3′G) (Pang et al., 2008), in which the sugar unit is attached to the 3′ hydroxyl group of the B-ring of the flavonoid instead of at the 3-*O*-position of the central heterocyclic C ring (Figure 1). UGT72L1 is preferentially expressed in the seed coat and is transcriptionally activated by the PA regulatory transcription factor *Arabidopsis* TT2 when this gene is expressed in *Medicago* hairy roots. The expression pattern of UGT72L1 in the seed coat correlates with the transient appearance of an epicatechin glucoside, levels of which decrease as oligomeric PA levels increase (Pang et al., 2008). These results are consistent with E3′G being a precursor of PAs in *Medicago* and, therefore, a likely substrate for transport to the vacuole. This series of experiments was therefore designed to identify the putative E3′G transporter in *Medicago*. Vacuole-enriched membrane vesicles from *Arabidopsis TT2*-expressing *Medicago* hairy roots take up E3′G in an ATP-dependent manner, and *Medicago* MATE1 was identified as a vacuolar E3′G transporter with a strong preference for E3′G over Cy3G. *Arabidopsis* TT12 was also shown to be an E3′G transporter. *Medicago MATE1* complements the *tt12* mutation in *Arabidopsis*, and genetic loss-of-function studies confirmed a role for MATE1 in PA biosynthesis in *Medicago*, further supporting the critical role of E3′G as a PA precursor.

RESULTS

Arabidopsis TT2 Induces Vacuolar Transport of E3′G in *Medicago* Hairy Roots

Ectopic expression of *Arabidopsis TT2* strongly activates transcription of *ANR* (for production of epicatechin) and *UGT72L1* in *Medicago* hairy roots, associated with transient production of E3′G and accumulation of PAs, whereas control *Medicago* hairy roots accumulate anthocyanin but not PAs (Pang et al., 2008). To determine whether *TT2*-mediated induction of PA biosynthesis is associated with enhanced transport of E3′G in the hairy roots, we first generated E3′G by incubation of (−)-epicatechin and uridine diphosphate glucose in the presence of recombinant UGT72L1 (Pang et al., 2008). The glucosylated product was isolated and purified, and its structure confirmed by nuclear magnetic resonance (NMR) analysis (Pang et al., 2008). We then isolated vacuole-enriched membrane vesicles from *TT2*-expressing and control hairy root tissues by differential centrifugation and sucrose gradient purification. Protein gel blot analysis of marker enzymes showed that the 20% sucrose and 20/30% sucrose interface fractions were enriched in vacuolar membranes (as seen by the higher level of the vacuolar H^+-ATPase marker, Figure 2A). The membrane vesicles from control hairy roots took up both Cy3G and daidzin, the 7-*O*-glucoside of the isoflavone daidzein, a known vacuolar component in *Medicago* roots (Naoumkina et al., 2007), in an ATP-dependent manner (Figures 2B and 2D; see Supplemental Figure 1 online) but did not take up E3′G (Figure 2C). However, vesicles from TT2-expressing hairy roots did exhibit ATP-dependent E3′G uptake as well as increased uptake of both Cy3G and daidzin (Figures 2B to 2D; see Supplemental Figure 1 online).

Concentration dependence studies of Cy3G and E3′G uptake into vacuolar membrane preparations from *Arabidopsis* TT2-expressing *Medicago* hairy roots indicated that E3′G and Cy3G uptake was saturable (Figures 2E and 2F). Double reciprocal plot analysis of initial rate data gave a K_m of 16.10 μM and V_{max} of 0.34 nmol/mg protein/min for E3′G uptake, with corresponding values of 49.10 μM and 4.23 nmol/mg protein/min for Cy3G. Uptake of Cy3G into vacuolar vesicles from vector control hairy roots was characterized by a K_m of 34 μM and V_{max} of 0.75 nmol/mg protein/min. Kinetic constants for daidzin uptake were similar (K_m 27.10 mM and V_{max} 0.83 nmol/min/mg protein). Overall, these results suggest that *Arabidopsis TT2* expression upregulates a high-affinity E3′G transporter and a lower affinity but higher capacity Cy3G transporter. The data also suggest that the transporter responsible for E3′G uptake is a different protein from the constitutively expressed Cy3G transporter(s).

Various inhibitors were used to further characterize the properties of the transporters responsible for uptake of Cy3G, E3′G, and daidzin in the *Medicago* hairy root membranes. When applied at appropriate concentrations in the uptake reaction, bafilomycin A1, a vacuole-type ATPase inhibitor (Drose and Altendorf, 1997), NH_4Cl, which dissipates the vacuolar membrane pH gradient (Rodrigues et al., 1999), and gramicidin D, a monovalent selective ionophore that dissipates the membrane potential and pH gradient (Luvisetto and Azzone, 1989), significantly inhibited Cy3G and E3′G uptake, whereas vanadate, a commonly used inhibitor of ABC transporters (Pezza et al., 2002), had almost no effect (Figure 2G). These data suggest that uptake of both Cy3G and E3′G into vacuoles is mediated by pH gradient-dependent H^+/antiporters. The observation that uptake of daidzin, but not of Cy3G or E3′G, was partially inhibited by vanadate (Figure 2G), suggests that daidzin uptake occurs by a mechanism distinct from that of Cy3G and E3′G uptake and may possibly involve an ABC transporter in addition to a pH gradient-dependent H^+/antiporter.

Competition assays showed that E3′G uptake into vacuolar membrane-enriched vesicles was slightly inhibited by Cy3G but not by various flavonoid aglycones, including free epicatechin and catechin (see Supplemental Figure 2 online). Likewise, Cy3G uptake was inhibited by E3′G but not by flavonoid aglycones or by isoflavone glucosides such as daidzin. Uptake of daidzin was, predictably, inhibited by genistin (genistein 7-*O*-glucoside), which differs from daidzin by the presence of a single hydroxyl group on the A-ring of the isoflavone moiety (see Supplemental Figure 2 online). Neither free epicatechin nor catechin was taken up by the membrane vesicles.

Identification of *Medicago* MATE1

The above-described uptake studies in *Medicago* root membrane vesicles predict the presence of a MATE transporter for vacuolar E3′G uptake in the model legume. The gene encoding this protein could be critical for engineering PA accumulation in

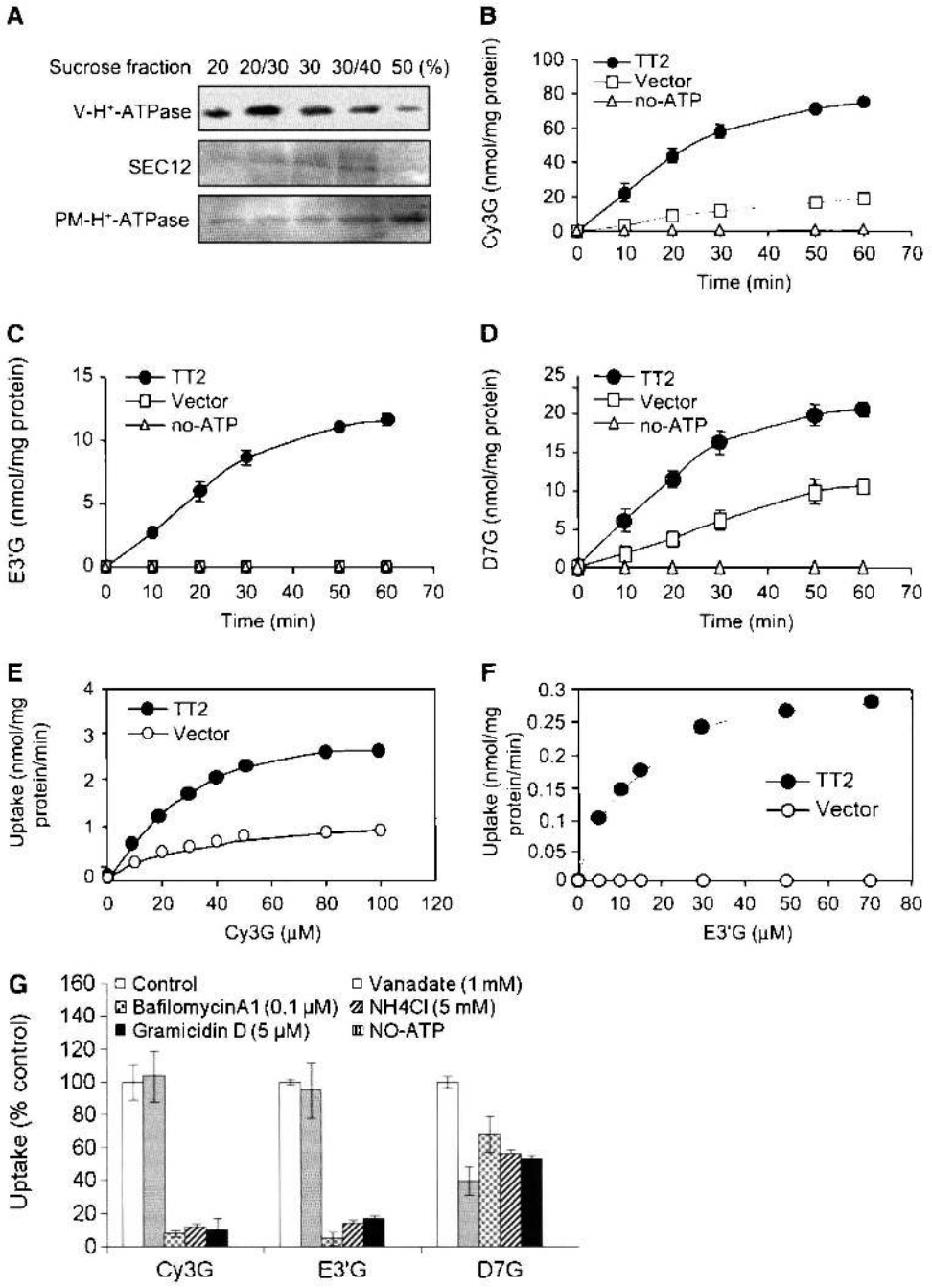

Figure 2. Uptake of Cy3G, E3'G, and Daidzin (D7) by Vacuole-Enriched Membrane Vesicles from *M. truncatula* Hairy Roots.

(A) Protein gel blot analysis of fractions from sucrose density gradients (numbers show percentage of sucrose, w/v) probed with antibodies against V-H^+-ATPase (vacuole marker), *Arabidopsis* SEC12 (endoplasmic reticulum marker), and PM-H^+-ATPase (plasma membrane marker).

(B) to **(D)** Time-dependent uptake of (iso)flavonoid glucosides into vacuole-enriched vesicles from hairy roots transformed with *Arabidopsis* TT2 (solid circles), empty vector (open squares), or TT2 but with no ATP in the uptake assay (open triangles). Substrate concentration was 50 μM. Results are mean and SD of three replicate uptake assays. D7G, daidzein 7-*O*-glucoside (daidzin).

(E) and **(F)** Concentration dependence of uptake of Cy3G and E3'G into membrane vesicles from hairy roots transformed with TT2 (solid circles) or empty vector (empty circles).

(G) Inhibition of Cy3G, E3'G, and D7G uptake (50 μM, 20-min assays) by inhibitors of membrane transport. Inhibitor concentrations were 1 mM (vanadate), 0.1 μM (bafilomycin A1), 5 mM (NH_4Cl), and 5 μM (gramicidin D). Results are mean and SD of five replicate uptake assays. No-ATP values are essentially zero.

forage legumes. No candidate gene was represented on the *Medicago* Affymetrix array previously used to study the *Arabidopsis* TT2-induced *Medicago* hairy root transcriptome (Pang et al., 2008). We therefore mined for *Medicago* MATE sequences using the *Arabidopsis* TT12 protein sequence to BLAST against the *M. truncatula* annotated genome protein database (http://biodecypher.noble.org/decypher/algo-tera-blast/tera-blastp_aa.shtml). Similar to *Arabidopsis*, which has 56 putative MATE transporters encoded in its genome, the *M. truncatula* genome sequence available to date contains >40 putative MATE-type transporters (see Supplemental Figure 3 and Supplemental Data Set 1 online). CT485797_21.5 (hereafter referred to as MATE1) is located on chromosome 5 and shares 70% identity and 80% similarity with *Arabidopsis* TT12 at the amino acid level (see Supplemental Figure 4A online). Phylogenetic analysis on available databases suggests that *Medicago* MATE1 is grouped into the same clade as *Arabidopsis* TT12 and TT12-like MATE transporters from several other species (Figure 3A). Most of these species, such as grapevine (*Vitis vinifera*) and poplar (*Populus trichocarpa*), produce high levels of PAs. *Arabidopsis* TT12 has been previously characterized as a Cy3G transporter but implicated in PA biosynthesis (Marinova et al., 2007), whereas CAO69962 from *V. vinifera* was suggested to be a putative PA precursor transporter based on microarray data from *V. vinifera* plants overexpressing the *Arabidopsis* TT2-like Myb transcription factors Vv MybPA1 and Vv MybPA2 (Terrier et al., 2009). CAO69962 transcripts (GSVIVP00018839001) were induced by these Myb transcription factors, coincidentally with other PA biosynthetic genes (Terrier et al., 2009). However, biochemical functions consistent with roles for *Arabidopsis* TT12 and the *V. vinifera* MATE transporter CAO69662 in PA biosynthesis have yet to be directly demonstrated. This group of MATE transporters related to PA accumulation is clearly distinct from the three known anthocyanin MATE transporters anthoMATE1 (AM1) and AM3 from *V. vinifera* and MTP77 from maize (*Zea mays*), as well as a nicotine MATE transporter from tobacco (*Nicotiana tabacum*; Figure 3A; see Supplemental Data Set 2 online) (Gomez et al., 2009; Morita et al., 2009; Shoji et al., 2009).

Protein structure prediction indicates that *Medicago* MATE1 and *Arabidopsis* TT12 have very similar secondary structures, each with 12 putative transmembrane domains (see Supplemental Figure 4B online).

Because *Medicago MATE1* probe sets were not present on the Affymetrix chip used for the previous analyses of *Arabidopsis* TT2-induced transcripts in *Medicago* hairy roots (Pang et al., 2008), quantitative RT-PCR (qRT-PCR) was used to examine *Medicago MATE1* expression. We used two transgenic hairy root lines that highly expressed *Arabidopsis TT2* and accumulated PAs and the corresponding vector control lines (Pang et al., 2008). *MATE1* expression was strongly induced in the two TT2-expressing lines but not in the vector control lines, in a similar manner to *ANR* expression (Figure 3B). However, another *Medicago* MATE transporter gene, *AC121237_16.5*, was not dramatically induced by AtTT2. qRT-PCR indicated that *MATE1* is predominantly expressed in flowers, young pods, and seed coats, with very low expression level in leaves, roots, petioles, stems, and vegetative buds (Figure 3C). *MATE1* expression increased in seedpods during the first 12 d after flowering and then decreased dramatically. Its transcript levels were low in mature seed coats. This expression pattern, which is similar to that of *TT12* in *Arabidopsis* siliques, parallels the expression patterns of previously identified *Medicago* PA biosynthesis-related genes, such as *ANR* and *UGT72L1* (Pang et al., 2008).

To examine the biochemical properties of MATE1, its open reading frame (ORF) was cloned from a cDNA library of young *M. trucatula* seedpods and expressed in yeast, both as the wild-type protein and as a fusion with the N terminus of the green fluorescent protein (GFP) ORF. Confocal microscopy indicated that the MATE1-GFP fusion protein localized to vesicle-like structures within the yeast cells (see Supplemental Figure 5 online). Uptake assays were then performed with microsomal fractions isolated from yeast cells expressing wild-type *Medicago* MATE1, MATE1-GFP fusion protein, or the empty vector (pYES) control. Time course and concentration dependence studies indicated that wild-type MATE1 transported E3′G at a higher velocity than Cy3′G (Figures 4A to 4D), and analysis of initial rate data at various substrate concentrations (Figures 4E and 4F) gave a K_m of 36.60 μM and V_{max} of 0.99 nmol/mg per min for transport of E3′G. Corresponding kinetic constants for Cy3G were 103.80 μM and 0.16 nmol/mg per min, respectively. The MATE1-GFP fusion protein was also functionally active (see Supplemental Figure 6A online).

Arabidopsis TT12 does not transport flavonol glycosides, such as quercetin or kaempferol 3-*O*-glucosides (Marinova et al., 2007). The same was true for *Medicago* MATE 1 when expressed in yeast (see Supplemental Figure 5C online); the yeast vesicles also failed to transport daidzein 7-*O*-glucoside or free epicatechin, catechin, or cyanidin (see Supplemental Figure 5C online). The uptake of E3′G by these vesicles was dependent upon the H^+ gradient, as determined by the inhibition of uptake by gramicidin D, NH_4Cl, and bafilomycin A1 (see Supplemental Figure 5B online).

Medicago MATE1 Is Localized to the Tonoplast Membrane

To determine the subcellular localization of the MATE1 protein, the 35S promoter-driven functionally active MATE1-GFP fusion was bombarded into tobacco leaf epidermal cells. A construct for transient expression of free GFP was used as control. MATE1-GFP fluorescence was detected only around the periphery of tobacco epidermal cells (Figures 5A, 5B, and 5G), quite different from the localization of free GFP, which shows strong cytosolic and plasma membrane signal, in addition to labeling of the nucleus (Figure 5D). MATE1-GFP could be visualized in a distinct line around the nucleus and in many small, fine vesicle-like structures that could potentially be prevacuolar (Figures 5A and 5G; see Supplemental Figures 7A to 7E online). A comparison with the localization of free GFP shows the clear lack of nuclear labeling with MATE1-GFP and the presence of the tonoplast membrane internal to the location of chloroplasts (Figures 5G to 5I). These features distinguish MATE1-GFP localization from that of plasma membrane–localized proteins (Lefebvre et al., 2004; Sutter et al., 2006).

To further confirm this observation, we examined the localization of the plasma membrane in the same cell types, using fluorescent dyes that are endocytosed into the membrane

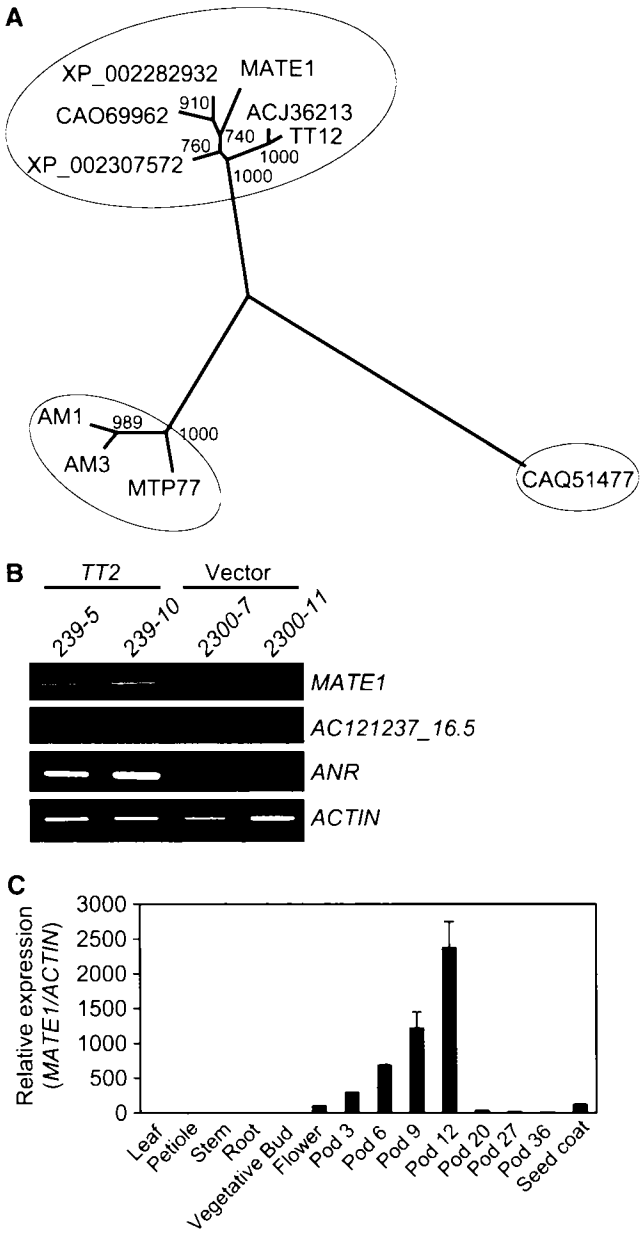

Figure 3. Phylogeny and Expression Pattern of *Medicago MATE1*.

(A) Phylogenetic tree of MATE transporters from different plant species. Protein sequences of the known anthocyanin MATE transporters *Arabidopsis* TT12, *V. vinifera* AM1 and AM3, *Zea mays* (maize) MTP77, a nicotine transporter from tobacco, and predicted MATE transporters XP_002282932 and CAO69962 from *V. vinifera*, XP_002307572 from *P. trichocarpa*, ACJ36213 from field mustard (*Brassica rapa*), and MATE1 from *M. truncatula* were aligned with ClustalW, and the nonrooted neighbor-joining tree was generated by the PAUP 4.0 program. Numbers at branch points indicate bootstrap support.

(B) Validation of *Medicago MATE1* expression in *TT2*-expressing *M. truncatula* hairy roots by RT-PCR. Expression of *TT2* also turns on the expression of *ANR*, but not of another *Medicago* MATE transporter gene, *AC121237_16.5*. Photos show representatives of three similar replicates.

(C) qRT-PCR analysis of the expression level (relative to *Medicago ACTIN*) of *MATE1* in different tissues of *M. truncatula*. Pods were analyzed at different times from 3 to 36 d after fertilization. Data are means and SD from three biological replicates.

(Emans et al., 2002). Plasma membrane labeled with the green fluorescent dye FM1-43 appeared as a highly uniform, sharp signal, with no evidence of labeling around the nucleus or on prevacuolar bodies (cf. Figures 5C and 5A). Furthermore, the membrane labeled with FM1-43 was outside the red fluorescent chloroplasts, as opposed to within them as observed for MATE1-GFP (cf. Figures 5G to 5I and 5J to 5L). Finally, we performed a comparative localization of MATE1-GFP fluorescence with the plasma membrane by labeling bombarded cells with the fluorescent marker FM4-64. A single cell expressing MATE1-GFP showed GFP signals in the tonoplast, around the nuclear membrane (long arrow), and in some of the prevacuole-like membrane vesicles (arrowheads) (Figure 5M); by contrast, FM4-64 label on the plasma membrane (red fluorescence in Figure 5N) only partially overlapped with that of MATE1-GFP on the inner side of the plasma membrane but not around the nucleus (long arrow) or on the prevacuole-like membrane vesicles (Figure 5O). These images suggest that MATE1-GFP is localized to the vacuolar membrane and are consistent with previous confocal images of tonoplast-targeted proteins, including TIPs and TT12-GFP (Hunter et al., 2007; Marinova et al., 2007).

Genetic Analysis of *MATE1* Function

A *Medicago* line harboring a Tnt1 retrotransposon insertion in the *MATE1* gene was isolated from the Noble Foundation's *M. truncatula* core Tnt1 mutant collection (Tadege et al., 2008). PCR with *Tnt1*- and *MATE1*-specific primers confirmed the insertion (in the 2nd exon of the gene) and the loss of *MATE1* transcripts in the plant (Figure 6A; see Supplemental Figure 8 online). F2 generation seeds of a homozygous line showed a clear *tt* phenotype, as indicated by the pale-colored seeds (Figure 6B). Staining whole seeds with dimethylaminocinnamaldehyde (DMACA), a reagent specific for PAs and their flavan 3-ol precursors (Li et al., 1996), confirmed that *mate1-1* seeds contain lower PA levels than wild-type seeds (Figure 6C). Analysis of cross sections through seeds indicated that DMACA-reactive material was virtually absent from the endothelial layer of seeds from the NF2629 line from the Noble Foundation's *Medicago* transposon insertion mutant collection (Figures 6D to 6H). Lack of PAs was confirmed by extraction and quantitative analysis of PAs from wild-type (R108) and mutant seeds (Figure 6I). Analysis of extracted soluble PAs by normal phase HPLC indicated that wild-type *M. truncatula* R108 contained a range of PA oligomers and polymers, whereas these were essentially lacking from the *mate1* mutant (Figures 6K and 6L). Prevention of E3'G transport in this line did not result in accumulation of epicatechin or E3'G (Figure 6L). Tnt1 insertion lines lacking *MATE1* expression showed normal expression of transcripts encoding the PA-specific gene *ANR* and the anthocyanin pathway genes *dihydroflavonol reductase* and *anthocyanidin synthase* (see Supplemental Figure 7 online), suggesting that the *tt* phenotype was due to a lack of precursor transport rather than to a lesion elsewhere in the pathway.

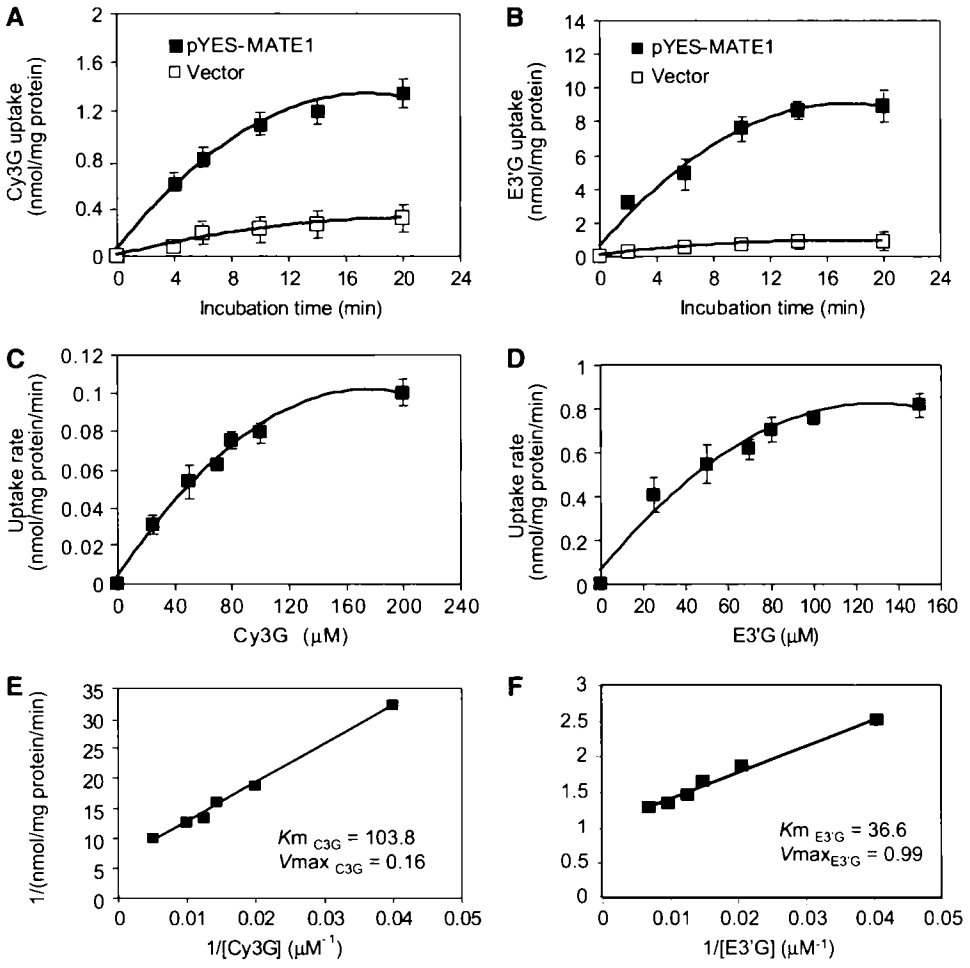

Figure 4. Uptake of Cy3G and E3′G by Yeast Microsomal Vesicles Expressing *Medicago* MATE1.

(A) and **(B)** Time-dependent uptake into vesicles from yeast cells transformed with MATE1 (closed squares) or empty vector (open squares). Substrate concentration was 100 μM. Results are mean and SD of three replicate uptake assays from three independent membrane preparations.
(C) and **(D)** Concentration dependence of uptake of Cy3G and E3′G into vesicles from yeast expressing MATE1.
(E) and **(F)** Double reciprocal plots of initial rate data at different concentrations of Cy3G and E3′G.

Arabidopsis TT12 Transports E3′G More Efficiently Than Cyanidin 3-*O*-Glucoside

Previous studies have shown that, when expressed in yeast, TT12 facilitates the vacuolar uptake of Cy3G and that this uptake is inhibited by C3G, which is not itself a substrate for transport (Marinova et al., 2007). Since *Arabidopsis* PAs are composed of epicatechin-type units like those of *M. truncatula*, and because we have recently demonstrated the formation of E3′G in *M. truncatula* (Pang et al., 2008) and shown that *Medicago* MATE1 is a transporter of E3′G, it was important to determine whether E3′G is also a preferred substrate for transport by *Arabidopsis* TT12. Using purified E3′G and commercial Cy3G as substrates, we conducted uptake assays with membrane vesicles isolated from yeast cells expressing either TT12 or empty vector control. Membrane vesicles from TT12-expressing yeast took up both E3′G and Cy3G when the compounds were present at 100 μM in the uptake mixture, whereas membrane vesicles from the vector control showed no uptake activity (Figures 7A and 7B). The initial rate of E3′G uptake was higher than that of Cy3G. Kinetic analyses revealed a K_m for E3′G uptake of 50.2 μM and a V_{max} of 0.73 nmol/mg protein/min; uptake of Cy3G by TT12 was less efficient, with a K_m of 293.6 μM and a V_{max} of 0.40 nmol/mg protein/min (calculated from Figures 7C and 7D). Cy3G inhibited E3′G uptake, but only at high concentrations relative to that of E3′G (Figure 7E), whereas E3′G inhibited Cy3G uptake at lower concentrations (see Supplemental Figure 9 online). In both cases, the competition was competitive.

As previously shown for Cy3G uptake (Marinova et al., 2007), TT12-mediated uptake of E3′G was sensitive to the vacuolar H^+ gradient dissipaters Bafilomycin A1 and NH_4Cl but not to the ABC transporter inhibitor vanadate, suggesting that an H^+/antiport mechanism is involved in the uptake (Figure 7F). Taken together, our results are consistent with E3′G being the preferred substrate for transport by TT12, a finding that explains the *tt*

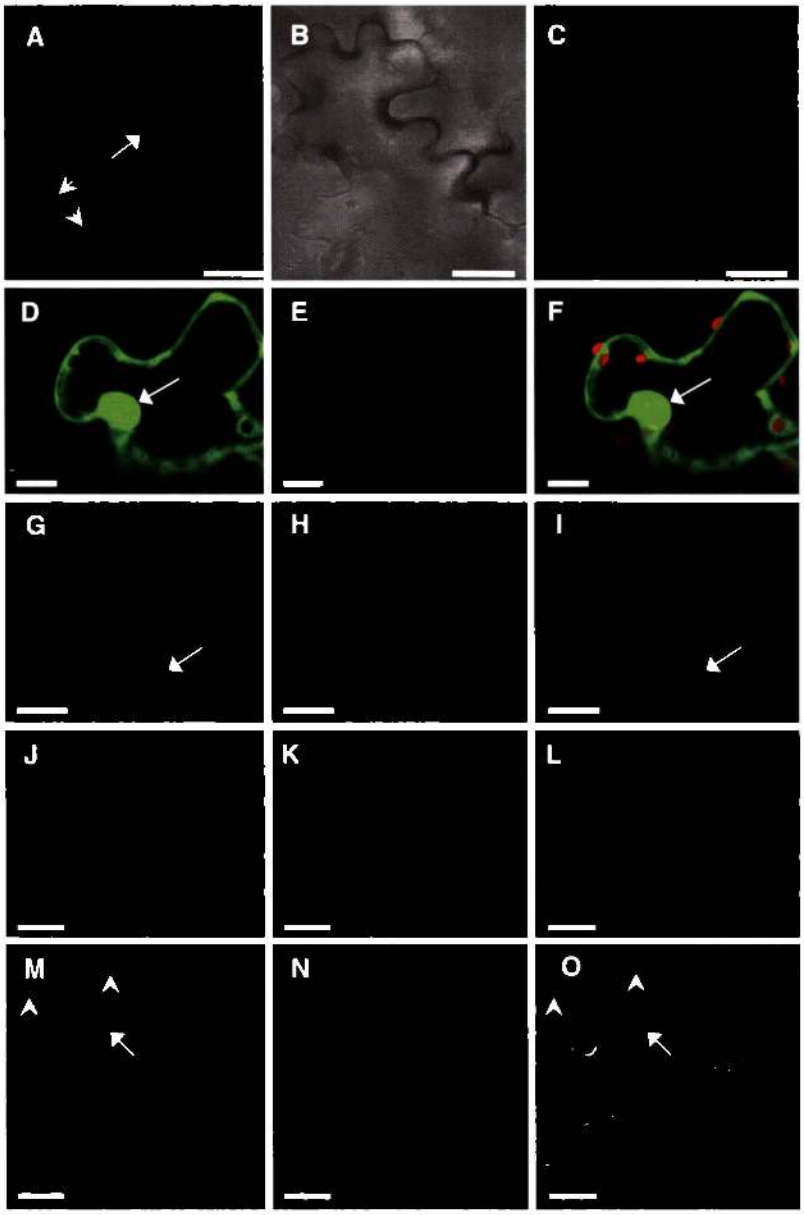

Figure 5. Subcellular Localization of MATE1-GFP.

MATE1-GFP driven by the cauliflower mosaic virus 35S promoter was transiently expressed in tobacco leaf epidermal cells and viewed by confocal microscopy.

(A) GFP fluorescence image of cells expressing MATE1-GFP. The large arrow shows the nucleus, and the arrowheads show prevacuolar or nuclear membranes. Bar = 50 μm.

(B) Differential interference contrast image of the same epidermal cell expressing MATE1-GFP as in **(A)**. Bar = 50 μm.

(C) FM1-43–labeled plasma membrane. Bar = 25 μm.

(D) to **(F)** Fluorescence images of a tobacco cell expressing free GFP. Bars = 20 μm.

(D) GFP fluorescence.

(E) Chloroplast autofluorescence image.

(F) Merged GFP image and chloroplast autofluorescence image. Arrow indicates the nucleus.

(G) to **(I)** Fluorescence images of a tobacco cell expressing MATE1-GFP. Bars = 20 μm.

(G) GFP fluorescence.

(H) Chloroplast autofluorescence image.

(I) Merged GFP image and chloroplast autofluorescence image. Arrow shows the position of the nucleus.

(J) to **(L)** Fluorescence images of a tobacco epidermal cell stained with the plasma membrane–specific dye FM1-43. Bars = 10 μm.

phenotype of the *TT12* knockout mutation (Debeaujon et al., 2001).

Complementation of the *tt12* Mutation by *Medicago MATE1*

To confirm that *Medicago MATE1* is a true functional ortholog of *Arabidopsis TT12*, we complemented the *Arabidopsis tt12* mutant by genetic transformation with a construct harboring the complete *MATE1* ORF. PCR screening identified >20 transgenic *tt12/MATE1* lines; three lines expressing *MATE1* transcripts were analyzed (Figure 8A). Comparison of seed coat phenotypes indicated restoration of seed coat color and DMACA staining as a result of expression of MATE1 in the *tt12* background (Figure 8B), and levels of soluble and insoluble PAs were restored to wild-type levels through complementation with *MATE1* (Figure 8C). *MATE1* complemented the loss of PA phenotype in the *tt12* background (Figures 8C and 8E) quantitatively (Figure 8C), but there were slight differences in size distribution between the PAs in wild-type Wassilewskija (Ws) and *tt12/MATE1* (Figures 8D and 8F) that were reproducible in the three independent lines. HPLC analysis of the PAs after acid-butanol hydrolysis confirmed that the extension units were derived wholly from (epi)catechin units in wild-type Ws and *tt12/MATE1* lines (see Supplemental Figure 8 online).

DISCUSSION

Medicago MATE1 and *Arabidopsis* TT12 Are E3′G Transporters

Previous studies have identified one *Arabidopsis tt* mutant, *tt12*, as defining a lesion in a MATE transporter involved in PA biosynthesis, and *tt12* plants show a defect in vacuolar PA accumulation in immature seeds (Debeaujon et al., 2001; Marinova et al., 2007). It was further shown that TT12 is localized to the tonoplast and can function as a transporter of Cy3G (Marinova et al., 2007). While the color of the seeds in *Arabidopsis* is attributed to accumulation of both anthocyanins and PAs (Routaboul et al., 2006), mature *tt12* seeds contain significantly lower levels of PAs and flavonols, such as quercetin-3-rhamnoside, but normal levels of anthocyanins (Marinova et al., 2007). Such phenotypes suggest that TT12 could function to specifically transport PA precursors into the vacuole (Marinova et al., 2007). However, biochemical studies in yeast showed that *Arabidopsis* TT12 can transport Cy3G, but not C3G or flavonol glucosides (Marinova et al., 2007), which does not explain why the *tt12* mutant has reduced PA accumulation. It was suggested that a glucoside of epicatechin might be the substrate transported by TT12 in vivo (Marinova et al., 2007).

We recently identified a seed coat–expressed UDP-glucosyltransferase acting specifically on epicatechin to produce the corresponding 3′-*O*-glucoside (Pang et al., 2008). Using the recombinant enzyme to produce this compound as a substrate for in vitro uptake studies, we have now shown that E3′G is efficiently transported by TT12 (Figure 7). An *M. truncatula* transporter protein (MATE1) sharing high sequence identity with TT12 was identified and shown to also transport E3′G and Cy3G. Both TT12 and MATE1 transport E3′G with higher affinity and velocity than Cy3G. MATE1 has a higher affinity and uptake velocity for transport of E3′G than does TT12, and the greater preference for E3′G compared with Cy3G is more apparent for MATE1 than for TT12.

Generally, flavonoids are transported in the form of glycosides. In the case of anthocyanidins, the first position to be glycosylated biosynthetically is the 3-*O*-position of the heterocyclic C-ring, and this stabilizes the highly reactive anthocyanidin molecule. It is interesting that TT12 and MATE1 transport both Cy3G and E3′G, although the latter is the kinetically preferred substrate (Figures 4 and 7). Clearly, the position of glycosylation is not critical for transport. One reason that C3G cannot be transported by TT12 (Marinova et al., 2007) may be that the *trans*-stereochemistry of catechin gives it a very different shape from that of 2,3-*cis*-epicatechin or the planar cyanidin. It is also possible that transport of Cy3G by TT12 and MATE1 simply reflects a relaxed specificity for binding of structurally related flavonoids that accommodates the planar anthocyanin molecule and that other transport systems, such as TT19 (Kitamura et al., 2004), or the endoplasmic reticulum-to-vacuole protein sorting route in *Arabidopsis* (Poustka et al., 2007) may represent the true physiological transporters for movement of anthocyanins to the vacuole. On the other hand, it is still not clear whether C3G occurs in planta, since so far there has, to the best of our knowledge, been no report of its isolation from plants. A biotransformation study showed that tobacco cells can transform both epicatechin and catechin into their 3′-*O*-glucosides (~38 to 46%), 5-*O*-glucosides (~7 to 10%), and 7-*O*-glucosides (~15 to 17%) (Shimoda et al., 2007). The study by Shimoda et al. (2007), together with our previous report that UTG72L1 catalyzes 3′-*O*-glycosylation of epicatechin (Pang et al., 2008), suggests that plant enzyme systems may preferentially glycosylate flavan-3-ols at the 3′-*O* position rather than the 3-*O* position favored for anthocyanin conjugation.

Figure 5. (continued).

(J) FM1-43 fluorescence.

(K) Chloroplast autofluorescence image.

(L) Merged image of FM1-43–labeled plasma membrane (green fluorescence) and chloroplasts (red autofluorescence).

(M) to **(O)** Fluorescence images of a tobacco epidermal cell expressing MATE1-GFP and stained with the plasma membrane–specific dye FM4-64. Bars = 25 μm.

(M) GFP fluorescence.

(N) FM4-64–labeled plasma membrane.

(O) Merged image of **(M)** and **(N)**. The arrows show the nucleus outside the vacuole, and the arrowheads show prevacuole-like vesicles.

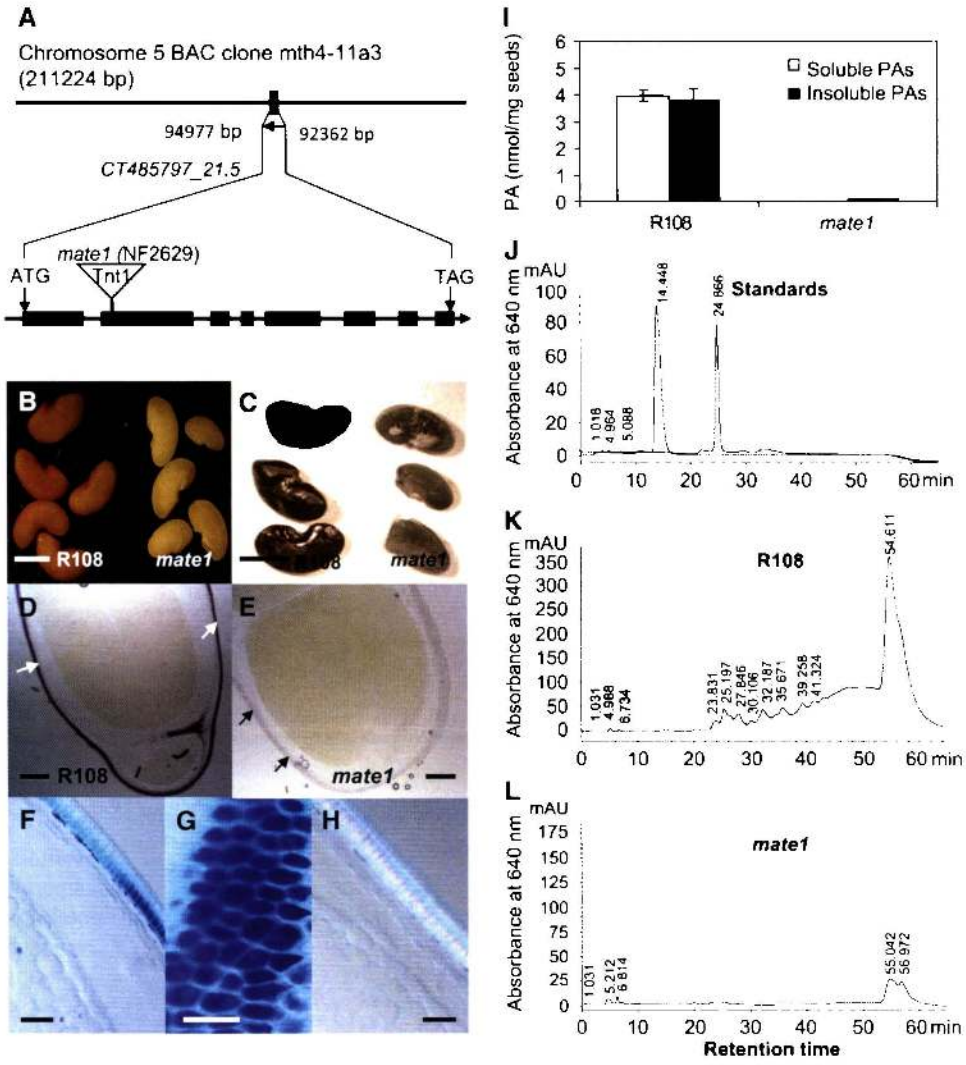

Figure 6. Loss-of-Function Analysis of *MATE1* in *M. truncatula*.

(A) The *MATE1* gene and the position of the Tnt1 retrotransposon insertion of line *mate1* (NF2629). Positions of introns (lines) and exons (black boxes) are shown.

(B) to **(E)** Seed phenotypes of wild-type *M. truncatula* R108 (left) and retrotransposon insertion line *mate1-1* (right).

(B) and **(C)** Whole seeds stained with DMACA in **(C)**. Bars = 2 mm.

(D) and **(E)** Cross sections of seeds stained with DMACA. Arrows show seed coats stained blue in R108 seed **(D)**, with almost no staining in the *mate1* seed **(E)**. Bars = 0.2 mm.

(F) to **(H)** Enlarged view of seed coat staining and cross section of stained seed coat cells showing location of PAs in the vacuoles. Blue color shows PA accumulation inside vacuoles. Bars = 40 μm.

(I) Levels of extractable PAs (soluble and insoluble) from seed of R108 and *mate1*. Values are mean and SD from three biological replicates.

(J) to **(L)** Analysis of size distribution of PAs in *Medicago* lines. Soluble PAs were resolved by normal phase HPLC with postcolumn derivatization with DMACA reagent and monitoring at 640 nm.

(J) Standards of monomer (catechin) and dimer (procyanidin B1).

(K) Soluble PAs from wild-type *M. truncatula* R108 seeds.

(L) PAs from the *M. truncatula* Tnt1 mutant *mate1*.

Neither epicatechin nor E3′G appear to accumulate in seeds of the *Arabidopsis tt12* mutant (Marinova et al., 2007) or in *mate1* (Figure 6). The reason for this is not clear at present, but the observation suggests that either these compounds are metabolized to other (non-PA) products in these mutants or that there is some feedback loop between transport and synthesis that blocks their formation. It is interesting that epicatechin does accumulate in the *aha10* mutant of *Arabidopsis*, which is also compromised in PA precursor transport (Baxter et al., 2005).

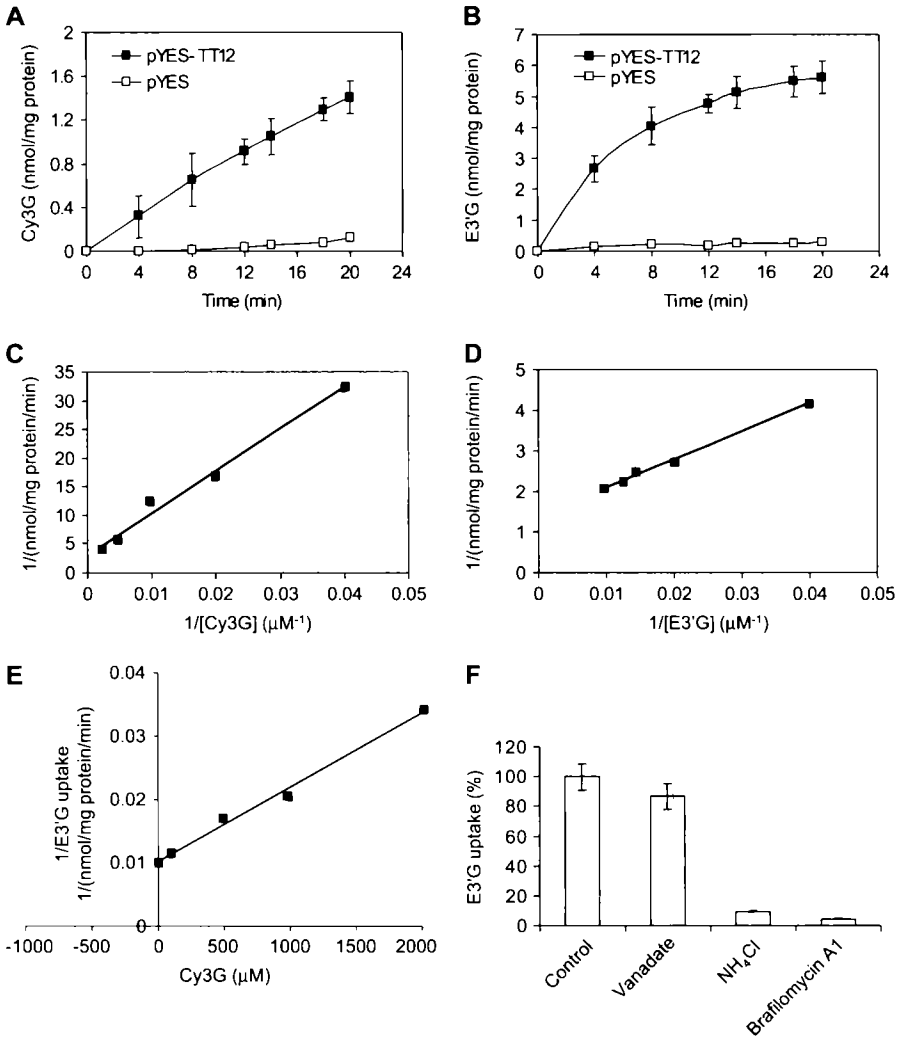

Figure 7. Uptake of Cy3G and E3'G by Yeast Microsomal Vesicles Expressing *Arabidopsis TT12*.

(A) and **(B)** Time-dependent uptake into vesicles from yeast cells transformed with TT12 (closed squares) or empty pYES vector (open squares). Substrate concentration was 100 μM. Results are mean and SD of at least three replicate uptake assays from three independent membrane preparations.

(C) and **(D)** Double reciprocal plots of initial rate data at different concentrations of Cy3G and E3'G.

(E) Plot showing inhibition of E3'G uptake by Cy3G.

(F) Inhibition of E3'G uptake (100 μM, 8-min assays) by inhibitors of membrane transport. Inhibitor concentrations were 1 mM (vanadate), 5 mM (NH_4Cl), and 0.1 μM (bafilomycin A1). Results are mean and SD from three replicate uptake assays.

TT2 Induces Flavonoid Transporters in *Medicago* Hairy Roots

Hairy roots of *M. truncatula* contain significant levels of anthocyanins and isoflavone glycosides, but no PAs. However, massive accumulation of PAs is induced in these roots by expression of the *Arabidopsis* MYB transcription factor TT2 (Pang et al., 2008). Consistent with these findings, vacuole-enriched membrane vesicle preparations from control hairy roots exhibit ATP-dependent uptake of both Cy3G and daidzein 7-*O*-glucoside, but not of E3'G. Vacuole-enriched vesicles from TT2 expressing roots take up all three compounds, with increased uptake of both Cy3G and D7G. Inhibitor studies suggest that the mechanism of uptake of D7G is different from that of Cy3G and E3'G, and most likely requires an ABC-type transporter, whereas the latter compounds are taken up by MATE-type transporters. ABC transporters have been identified as an important class of transporters for plant secondary metabolites (Yazaki, 2005; Kitamura, 2006) and are involved, for example, in the secretion of the isoflavone genistein from soybean (*Glycine max*) roots (Sugiyama et al., 2007). Our results indicate that vacuolar E3'G uptake is dependent on expression of a PA regulatory transcription factor and that there is more than one transporter for Cy3G, as suggested above. One Cy3G transporter is constitutively expressed in the hairy roots,

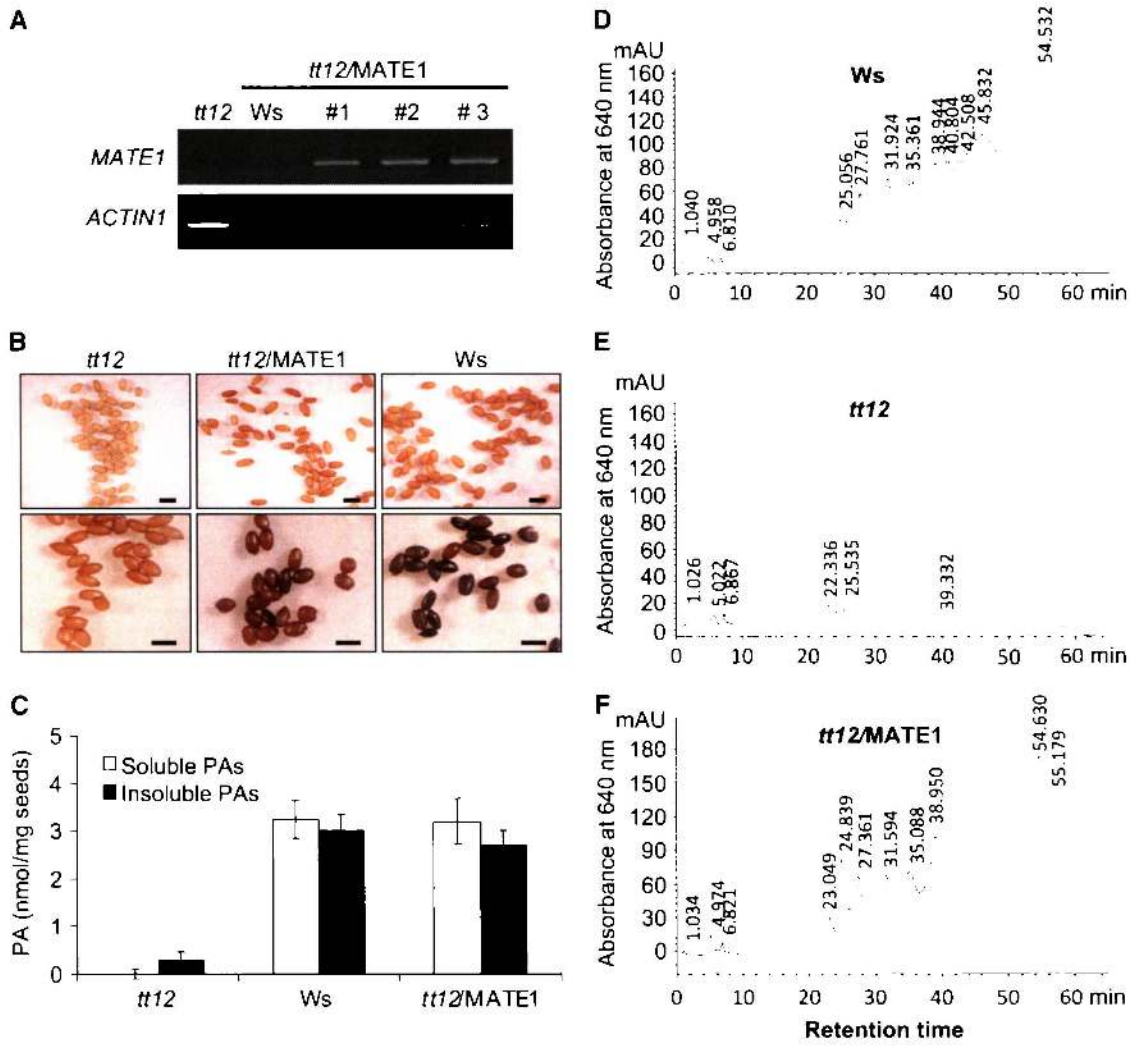

Figure 8. Complementation of the *Arabidopsis tt12* Mutation by *Medicago MATE1*.

(A) RT-PCR screening to indicate the presence of *Medicago MATE1* transcripts in three independent *Arabidopsis* transformants. *Arabidopsis ACTIN* expression was used as an internal control.

(B) Seed phenotypes of the *tt12* mutant, wild-type *Arabidopsis* ecotype Ws, and *tt12* complemented with *MATE1*. The three bottom panels show seed after staining with DMACA. Bars = 0.3 mm.

(C) Levels of extractable PAs (soluble and insoluble) from seeds of the *tt12* mutant, wild-type *Arabidopsis* ecotype Ws, and *tt12* complemented with *MATE1*. Values are mean and SD from three biological replicates.

(D) to **(F)** Soluble PA size distribution in seeds of *Arabidopsis*. Soluble PAs were resolved by normal-phase HPLC with postcolumn derivatization with DMACA reagent and monitoring at 640 nm.

(E) PAs from wild-type Ws seeds.

(F) PAs from *tt12* seeds.

(G) PAs from *tt12/MATE1* seeds.

and another is induced by *Arabidopsis* TT2. The Cy3G transport induced by TT2 may result from the activity of MATE1, which nevertheless shows a kinetic preference for the uptake of E3′G.

Modification of flavonoids and other compounds by processes such as glycosylation and acylation is often a necessary prerequisite for their transport into the vacuole by MATE or ABC transporters (Klein et al., 1996; Bartholomew et al., 2002; Marinova et al., 2007; Gomez et al., 2009), and flavonoid aglycones are generally not suitable substrates for MATE transporters. *Arabidopsis* TT12 transports Cy3G but not C3G, flavonoid aglycones, or flavonol glucosides, such as quercetin-3-*O*-glucoside (Marinova et al., 2007). Grape anthoMATE1 transports acylated anthocyanins, but not nonacylated anthocyanins, into the vacuole (Gomez et al., 2009). However, a MATE transporter from tobacco can transport nonmodified nicotine directly into the vacuole (Morita et al., 2009; Shoji et al., 2009). *Medicago* MATE1 preferentially transports E3′G over Cy3G and does not transport daidzin (an isoflavone glucoside) or flavonoid

aglycones (see Supplemental Figure 6 online). Overall, these studies indicate that some MATE transporters exhibit a degree of substrate specificity. Such specificity may have important physiological consequences during seed development and PA biosynthesis. A low level of epicatechin glucoside has been detected in *Arabidopsis* seeds (Marinova et al., 2007), and developing *Medicago* seeds accumulate E3′G up to 0.4 nmol per mg fresh weight of seed coat at 12 d after pollination (Pang et al., 2008). E3′G is therefore likely to be preferentially transported into the vacuole at the expense of Cy3G transport by TT12 or MATE-1 during PA accumulation.

MATE1 Is Required for PA Biosynthesis in *Medicago*

Reverse genetic screening led to the identification of one *M. truncatula* line with a Tnt-1 retrotransposon insertion in the *MATE1* gene. Seeds of this line exhibited a *tt* phenotype similar to that of *Arabidopsis tt12* (Debeaujon et al., 2001), and metabolite analysis confirmed that *mate1* seeds have drastically reduced PA levels. Other genes of PA biosynthesis were not downregulated in *mate1*, suggesting that it is the insertion in the *MATE1* gene that confers the loss of PA phenotype. The in vivo function of *MATE1* was confirmed by complementation of the *Arabidopsis tt12* mutant. Interestingly, PA production was restored quantitatively, but there were small differences in PA quality as regards polymer size distribution on comparing wild-type *Arabidopsis* Ws and *tt12* expressing *Medicago MATE1* (Figures 8D and 8F) The reason for this is not clear at present. Clearly though, *MATE1* is a functional ortholog of *TT12*. Recently, several different MATE-type transporters have been reported to participate in vacuolar sequestration of various secondary metabolites (Yazaki, 2005; Marinova et al., 2007; Morita et al., 2009; Shoji et al., 2009), suggesting that this class of transporters may be generally involved in transport of plant secondary metabolites into the vacuole.

As a plant secondary transporter, *Medicago* MATE1 requires an electrochemical H^+ gradient across the vacuolar membrane for transport of E3′G or C3G, with the downhill force of the H^+ gradient between the vacuole and the cytosol. Although it is well known that V-ATPase and pyrophosphatase generally provide the H^+ gradient across the vacuolar membrane (Gaxiola et al., 2002), there is no report so far that these proteins are involved in PA biosynthesis. By contrast, the *Arabidopsis* H^+ ATPase 10 (AHA10), an annotated plasma membrane protein, has been shown to be necessary for PA production in *Arabidopsis* seeds (Baxter et al., 2005). It has been suggested that AHA10 may either be involved in vacuolar acidification to energize TT12 as a PA precursor transporter or in transport of PA precursors through vesicle trafficking, since the localization of AHA10 has not been resolved (Baxter et al., 2005; Marinova et al., 2007). Interestingly, a recent study shows that hybrid petunia (*Petunia* × *hybrida*) PH5, a putative ortholog of AHA10, is involved in flower color determination and PA production in seeds (Verweij et al., 2008); moreover, PH5 is localized to the tonoplast and believed to acidify the vacuole to enhance anthocyanin coloration and, probably, PA precursor loading into the vacuole (Verweij et al., 2008). Therefore, it is possible that AHA10 is also localized to the vacuolar membrane.

At least 40 other MATE transporters are present in the *Medicago* genome. Because the PAs of both *Medicago* and *Arabidopsis* are somewhat unusual in containing only epicatechin units (Lepiniec et al., 2006; Pang et al., 2007), *Medicago* MATE1 and *Arabidopsis* TT12 may be the only transporters necessary for PA biosynthesis in these species, unless the epicatechin-terminal and extension units in PAs have different biosynthetic origins (see below). Our studies with *M. truncatula* are ultimately targeted toward improvement of alfalfa (*Medicago sativa*), and this species has been reported to possess seed coat PAs with catechin-terminal units and epicatechin (major) and epigallocatechin (minor) extension units (Koupai-Abyazani et al., 1993). Studies to determine whether *Medicago* MATE1 or related transporters from alfalfa can facilitate uptake of catechin and epigallocatechin glucosides are in progress.

Unresolved Questions Concerning PA Monomer Transport

The results in this article define the biochemical functions of *Arabidopsis* TT12 and its putative ortholog from *M. truncatula*. E3′G, formed in *Medicago* by glycosylation of the product of the ANR reaction by UGT72L1, is transported to the vacuole for subsequent use in PA biosynthesis. However, what happens next is still far from clear because the nature of the condensing units in PA biosynthesis has yet to be determined. It is generally believed that the terminal catechin or epicatechin units of PAs originate from free catechin or epicatechin (Marles et al., 2003), and conversion of E3′G back to the flavanol aglycone could easily be accomplished by the activity of a vacuolar glucosidase. Indeed, a glucosidase is induced over threefold by TT2 in *M. truncatula* hairy roots (Pang et al., 2008), but its intracellular localization and biochemical activity remain to be determined. The nature of the condensing units is more problematical. The long-held model based on nonenzymatic chemical synthesis of PAs at low pH places leucoanthocyanidin as the condensing unit (Marles et al., 2003), but this seems unlikely since this compound has 2,3-*trans* stereochemistry and cannot therefore account for epicatechin-type extension units (Marles et al., 2003; Xie and Dixon, 2005; He et al., 2008). Alternative models have been proposed in which epicatechin, or some derivative of epicatechin, is oxidized to yield a corresponding quinone methiode or carbocation, which then attacks the 8-position of the A-ring of the (epi)catechin-terminal unit to extend the chain (Xie and Dixon, 2005; He et al., 2008). Such a model would only require transport of epicatechin units to the vacuole. However, similar reactive intermediates could be generated from achiral cyanidin derivaties (Marles et al., 2003; Xie and Dixon, 2005), consistent with a role for an additional anthocyanin transporter, such as TT19, which appears to function in both PA precursor and anthocyanin transport in *Arabidopsis* (Kitamura et al., 2004). It seems unlikely that TT12 or MATE1 would transport both Cy3G and E3′G into seed coat vacuoles in parallel because high concentrations of E3′G would inhibit transport of Cy3G (see Supplemental Figure 9 online), and an inverse relationship between expression of ANR and anthocyanidin 3-*O*-glucosyltransferase has been demonstrated and proposed to result in selective direction of cyanidin into either PA or anthocyanin biosynthesis (Lee et al., 2005).

Finally, our studies, although establishing the involvement of a MATE transporter in PA monomer transport, do not exclude

the possibility that membrane vesicle-mediated transport of flavonoids (Grotewold, 2004; Poustka et al., 2007) may also be involved in PA biosynthesis and accumulation. Further experimentation will be necessary to confirm whether the vesicle-like structures that label with MATE1-GFP (see Supplemental Figure 7 online) are indeed destined for the vacuole.

METHODS

Plant Materials, *Medicago truncatula* Tnt1 Mutant Screening, and Growth of Hairy Roots

Seeds of *Medicago truncatula* line R108 were scarified with concentrated sulfuric acid, rinsed, sterilized with 2% sodium hypochlorite, and vernalized at 4°C for 3 d on moist, sterile filter paper. Germinated seedlings were transplanted to pots containing soil and placed in a greenhouse set to the following conditions: 16-h/8-h light/dark regime, 200 $\mu E\ m^{-2}\ s^{-1}$ light irradiance, 24°C, and 40% relative humidity. Reverse genetic screening of *M. truncatula* Tnt1 mutants in the R108 background was performed as described previously (Peel et al., 2009). For identification of the *Tnt1* insertion mutant for *Medicago MATE1*, PCR amplification was performed using a combination of *MATE1*-specific primers and *Tnt1*-specific primers (see Supplemental Table 1 online), and the PCR products were fully sequenced.

Growth of *Arabidopsis thaliana TT2*-expressing *M. truncatula* hairy roots was as described previously (Pang et al., 2008). Both *TT2*-expressing and empty vector control hairy root lines were used for isolation of microsomal fractions and preparation of vacuolar membrane-enriched vesicles.

Complementation of the *Arabidopsis tt12* Mutant

The ORF of *Medicago MATE1* in the binary vector pB2GW7 was driven by the 35S cauliflower mosaic virus promoter and terminated by the NOS terminator. Both pB2GW7-MtMATE1 and empty pB2GW7 vector (control) were transformed into *Agrobacterium tumefaciens* strain LBA4404 using the electroporation method. Transformed colonies were grown on YEP medium with selection at 28°C for transformation of *Arabidopsis tt12* flowers using the floral dip infiltration method (Clough and Bent, 1998). *Arabidopsis tt12* mutant in the Ws background (kindly provided by Isabelle Debeaujon, Jean-Pierre Bourgin Institute, Institut National de la Recherche Agronomique, France) and wild-type Ws plants were grown in a growth chamber at 20 to ~22°C, 100 $\mu E\ m^{-2}\ s^{-1}$ light intensity provided by cold fluorescent tubes with a 18/6-h light/dark period. The F1 transgenic plants were selected with phosphinothricin (7.5 μg/mL) and kanamycin (20 μg/mL) on one-half Murashige and Skoog plates. F2 generation plants with confirmed *MATE1* expression were used for analysis of seed phenotype and PA levels in seeds.

Gene Cloning and Vector Construction

Arabidopsis TT12 cDNA was cloned from a cDNA library constructed from young wild-type (Columbia-0) *Arabidopsis* siliques (4-week-old plants, 1 to 5 d after flowering) with a forward primer and a reverse primer that enable PCR fragments to be directionally cloned into pENTR vector (see Supplemental Table 1 online). *MATE1* was cloned from cDNA constructed from young pods (9 to 12 d after flowering) of *M. truncatula* wild-type (R108) plants. Total RNA was extracted from *Arabidopsis* siliques or *M. truncatula* seedpods using the RNeasy plant mini kit procedure (Qiagen). First-strand cDNA was synthesized from total RNA with the SuperScript III first-strand synthesis system (Invitrogen) according to the manufacturer's protocol. The *MATE1* ORF was amplified with MtMATE1-5′ forward primer and MtMATE1-3′ reverse primer (see Supplemental Table 1 online). The PCR products were cloned into the pENTR/D-TOPO vector (Invitrogen) for sequencing, and the confirmed clone was subcloned into Gateway destination vectors, the yeast expression vector pYES (uracil selection marker), or the plant binary vector pB2GW7 by recombination using Gateway LR Clonase (Invitrogen).

The MATE1-GFP fusion was constructed by cloning the *MATE1* ORF in frame with the N terminus of GFP. The *MATE1* ORF was amplified with a pair of primers, MtMATE1-GFP-5′ and MtMATE1-GFP-3′ (see Supplemental Table 1 online). PCR products were subcloned into a yeast GFP cassette shuttle vector fusion in frame to the N terminus of GFP. The construct pHGDP-MtMATE1-GFP was transformed into yeast cells for testing MATE1-GFP expression. A 2.1-kb MATE1-GFP coding sequence was then amplified with the primer pair MtMATE1 SFI-5′ and MtMATE1 SFI-3′ (see Supplemental Table 1 online) and subcloned into the pENTR/D-TOPO vector, followed by subcloning into the plant binary vector pB2GW7 by recombination with Gateway LR Clonase. The 35S:MATE1-GFP construct was used for localization studies. All clones were confirmed by sequencing.

Chemicals and Reagents

Flavonoid aglycones, cyanidin 3-*O*-glucoside, and daizein 7-*O*-glucoside (daidzin) were obtained from Indofine Chemical Company. E3′G was purified from incubation of epicatechin with recombinant UGT71G1 as described previously and its structure confirmed by NMR spectroscopy (Pang et al., 2008).

Yeast Culture, Transformation, and Microsomal Fraction Preparation

Saccharomyces cerevisiae strain W303A (*Matα ade2-1 ura3-1 his3-11,15 trp1-1 leu2-3,112 can1-100*) (kindly provided by Kendal Hirschi at Baylor College of Medicine) was used to express *Arabidopsis* TT12 and *Medicago* MATE1 transporter. The Gateway yeast expression vectors pYESDEST (Invitrogen) and pYES harboring TT12 or MATE1 were transformed into W303A by the polyethylene glycol/lithium acetate method. Transformants were grown in YNB (−uracil) + galactose medium overnight at 30°C and then transferred to 500 mL YPD medium at 30°C for overnight growth. Yeast cells were collected for microsomal extraction as described previously (Nakanishi et al., 2001). Briefly, cells were collected by centrifugation at 3000*g* and washed once with 0.1 M Tris-HCl, pH 9.4, 50 mM 2- mercaptoethanol, and 0.1 M glucose. Cells were then digested with zymolyase medium (50 mM Tris-MES, pH 7.6, 0.9 M sorbitol, 0.1 M glucose, 5 mM DTT, and Zymolyase [Seikagaku Corporation]) at 30°C for 2 h with gentle agitation. Spheroplasts were collected by centrifugation at 3000*g* for 10 min and washed with 1 M sorbitol. The spheroplasts were resuspended in 50 mM Tris-MES, pH 7.6, 1.1 M glycerol, 1.5% polyvinylpyrrolidone, 5 mM EGTA-Tris, 1 mM DTT, 0.2% BSA, 1 mM phenylmethylsulfonyl fluoride (PMSF), and 1 mg/liter leupeptin and then homogenized with a motor-driven Teflon homogenizer. After centrifugation at 2000*g* for 10 min, the precipitate was washed with the same buffer and centrifuged again. All of the supernatant fractions were pooled and centrifuged at 120,000*g* for 30 min. The pellets were suspended in 5 mM Tris-MES, pH 7.6, 0.3 M sorbitol, 1 mM DTT, 0.1 M KCl, and protease inhibitor cocktail (10 μg/mL leupeptin, 2 μg/mL aprotinin, 2 μg/mL pepstatin, 1 mM PMSF, and 1 mM EDTA). The suspension was stored at −80°C until use.

Preparation of Membrane Vesicles from Hairy Roots

Vacuolar membrane vesicles were prepared from hairy roots of *M. truncatula* essentially according to the method described previously (Zhao et al., 2009). All procedures were performed on ice or at 4°C unless otherwise stated. Hairy roots were homogenized in ice-cold

homogenization buffer containing 100 mM Tris-HCl, pH 7.6, 10% (v/v) glycerol, 0.5% (w/v) polyvinylpolypyrrolidone, 5 mM EDTA, 150 mM KCl, 5 mM DTT, and 2 mM PMSF. The homogenate was strained through Miracloth (Calbiochem) and centrifuged at 10,000*g* for 10 min. The resulting supernatant was centrifuged at 100,000*g* for 40 min. The pellet was resuspended in buffer containing 20 mM Tris-HCl, pH 7.6, 10% (v/v) glycerol, 1 mM DTT, and protease inhibitor cocktail (Sigma-Aldrich). The suspension was layered over a 20% to 30% to 40% to 50% (w/v, in 20 mM Tris-HCl buffer, pH 7.6, 1 mM DTT, and 1 mM EDTA) discontinuous sucrose gradient in a 13-mL tube. The tubes were subjected to centrifugation at 100,000*g* for 180 min. Fractions recovered from the interfaces were resuspended in ~35 mL of resuspension buffer and centrifuged at 100,000*g* for 40 min. Each pellet was resuspended in resuspension buffer supplemented with protease inhibitor cocktail and stored at −80°C until use. Vacuole-enriched membrane vesicles were present in the 20% and 20/30% interface fractions, as determined by protein gel blot analysis with antibodies against marker proteins.

Transport Activity Assays

The measurement of uptake by vacuolar membrane vesicles was performed at 25°C by a method modified from that of Bartholomew et al. (2002). The 600- to 1000-μL assay mixtures contained 25 mM Tris-MES, pH 8.0, 0.4 M sorbitol, 50 mM KCl, 5 mM Mg-ATP, 0.1% (w/v) BSA, and the indicated concentrations of transport substrate. ATP was omitted from the nonenergized controls. Assays were initiated by the addition of membrane vesicles (~50 μg of protein) and brief agitation. Batches of the reaction mixture (100 μL) were removed at various times, and their reactions terminated with 1.0 mL of ice-cold washing solution (25 mM Tris-MES, pH 8.0, containing 0.4 M sorbitol). The mixtures were then subjected to vacuum filtration through prewetted GV Durapore polyvinylidene difluoride membrane filters (0.2-μm pore diameter; Millipore). The dried filters were transferred to 20-mL glass vials containing 1.0 mL of 50% (v/v) methanol. The vials were capped and the filters were extracted for 1 h at room temperature in an orbital shaker. The eluate was analyzed by HPLC.

For inhibitor assays, transport inhibitors were incubated with the membrane vesicles at the following final concentrations: 1 mM vanadate, 5 mM gramicidin D, 0.1 mM bafilomycin A1, or 5 mM NH_4Cl. The inhibitors were added to the reaction mixtures 2 min prior to initiation of uptake reactions by addition of substrate. Transport inhibitors were prepared in stock solutions of 1 M vanadate in water, 5 mM bafilomycin A1 in DMSO, 5 mM gramicidin D (in DMSO), and 1 M NH_4Cl in water.

For competition assays with hairy root membrane vesicles, 10 mM stock solutions of epicatechin, catechin, genistein, daidzin, daidzein, E3′G, and Cy3G were prepared in 50% DMSO or methanol. Flavonoid aglycones or glucosides were added to the reaction mixture at a final concentration of 250 μM, while the uptake substrate concentration was set at 50 μM. For competition assays with yeast membrane vesicles expressing *Arabidopsis* TT12, various concentrations of Cy3G were used with E3′G as substrate at 100 μM. After incubation at 25°C for 10 min, transported E3′G was measured by HPLC. Reverse-phase HPLC analyses were performed on an Agilent HP1100 HPLC using a gradient mobile phase: solvent A (1% phosphoric acid) and B (acetonitrile) at 1 mL/min flow rate: 0 to 5 min, 5% B; 5 to 10 min, 5 to 10% B; 10 to 25 min, 10 to 17% B; 25 to 30 min, 17 to 23% B; 30 to 65 min, 23 to 50% B; 65–79 min, 50 to 100% B; 79 to 80 min, 100 to 5% B. Data were collected at 206 and 530 nm for epicatechin and cyanidin derivatives, respectively. Identifications were based on chromatographic behavior and UV spectra compared with those of authentic standards.

Determination of Transport Kinetics

Transport assays were performed with different concentrations of E3′G, Cy3G, and daidzin (from 25 to 200 μM) and 5 mM MgATP. After incubation at 25°C for 10 min, transported glycosides were measured by HPLC as described above. Lineweaver-Burk plots were used to calculate K_m and V_{max} values.

Protein Gel Blot Analysis

For immunoblotting, ~10 μg of vacuolar membrane vesicle proteins were denatured in protein loading buffer at 98°C for 5 min, subjected to SDS/7 to 12% PAGE (Bio-Rad), and transferred to polyvinylidene difluoride membrane. The membrane was blocked with 5% nonfat milk, incubated with primary antibodies and secondary horseradish peroxidase–conjugated anti-rabbit IgG antibodies, and then subjected to immunodetection with a WesternBreeze Chemiluminescent Immunodetection Kit (Invitrogen) according to standard procedures. Antibodies used for immunodetection were against plasma membrane H^+-ATPase and endoplasmic reticulum marker SEC12 (Sar1p exchange factor 12) (kindly provided by Rujin Chen, Noble Foundation) and vacuolar V-type H^+-ATPase (subunit E) from *Arabidopsis* (Agrisera AB; used at 1:1000 dilution).

Light and Confocal Microscopy

Seeds of *M. truncatula* wild-type R108 and Tnt1 insertion mutant *mate1-1*, as well as *Arabidopsis* Ws, *tt12*, and tt12/MtMATE1, were imaged before and after DMACA staining. Seeds were stained with 2% (w/v) DMACA in 3 M HCl/50% methanol (v/v) for 4 d and washed three times with 70% ethanol for 2 d (Abrahams et al., 2002). An Olympus SZX12 fluorescence microscope with a Spot RT color camera run by Spot Basic and Spot Advanced software was used to visualize seeds. For visualizing DMACA-stained seed cross sections, seeds were quickly frozen in liquid nitrogen and processed with a Cryostat Leica CM 1850 Microtome into 20-μm sections for observation under a Nikon SMZ1500 fluorescence microscope installed with a Nikon DXM 1200 run by ACT-1 software.

Five micrograms of plasmid DNA containing *35S:MATE1-GFP* or *35S:GFP* was mixed with 20 μL of an aqueous suspension containing 1.0-μm gold particles. After washing, the gold was spread onto plastic carrier discs for biolistic bombardment of tobacco epidermal cells using a Bio-Rad 1000/HE particle delivery system. After 16 to 48 h, epidermal cells of tobacco leaves were viewed directly with a Leica TCS-SP2 AOBS confocal laser scanning microscope (Leica Microsystems) to examine the localization patterns of MATE1-GFP. GFP was excited using the 488-nm line of the argon laser and emission was detected at 520 nm.

To compare the difference between MATE1-GFP–labeled tonoplast and the plasma membrane, a styryl FM dye FM1-43 (*N*-(3-triethylammoniumpropyl)-4-(4-[dibutylamino]styryl)pyridinium dibromide) was used to label the plasma membrane (Emans et al., 2002). Tobacco leaf strips were incubated in a 10 μM aqueous solution of FM1-43 for 10 min and then observed under the confocal microscope. FM1-43 was excited at 488 nm and emission was detected at 560 nm. Chloroplasts were visualized at 560 to 610 nm under excitation at 543 nm.

To further distinguish MATE1-GFP signal from the plasma membrane signal, tobacco leaf epidermal cells expressing MATE1-GFP were stained with a 10 μM aqueous solution of the dye FM4-64 for 10 min before being observed under the confocal microscope. FM4-64–labeled plasma membrane was excited at 543 nm with the argon laser and emission was detected from 620 to 680 nm.

All images were acquired at a resolution of 512 × 512 pixels using a ×60/1.20 water-immersion objective and analyzed with Leica LAS AF software.

qRT-PCR

For testing expression of *MATE1* and *ANR* in hairy roots, total RNA was isolated from *M. truncatula* hairy roots expressing *Arabidopsis* TT2 or

β-glucuronidase (control) using the RNeasy plant mini kit (Qiagen) for cDNA synthesis. Equal amounts of total RNA were treated with DNaseI (Invitrogen) and were subsequently heat inactivated. cDNAs were synthesized with the SuperScript III first-strand synthesis system (Invitrogen). Diluted fractions were used for PCR (Promega; Mixgo polymerase). *Medicago MATE1*, *ANR*, and *ACTIN* were amplified in 25 cycles (94°C for 30 s, 55°C for 30 s, and 72°C for 30 min). Primers are shown in Supplemental Table 1 online.

For q-RT-PCR, cDNA from *M. truncatula* tissues was prepared as previously described (Benedito et al., 2008). Pods were collected at different times from 3 to 36 d after fertilization for cDNA synthesis. Seed coat RNA was isolated from seeds at 12 d after pollination (Pang et al., 2008). qPCR was performed with an ABI PRISM 7900 HT sequence detection system (Applied Biosystems). Reactions contained 2.5 μL of SYBR Green Master Mix reagent (Applied Biosystems), 0.5 μL of cDNA, and 200 nM of each gene-specific primer in a final volume of 5 μL and underwent 40 cycles of amplification. Data were analyzed using the SDS 2.2.1 software (Applied Biosystems). PCR efficiency (E) was estimated using the LinRegPCR software (Ramakers et al., 2003), and the transcript levels were determined by relative quantification (Pfaffl, 2001) using the *Medicago ACTIN* gene as a reference.

Quantitative Analysis of PAs

Extraction and subsequent analysis of total soluble and insoluble PAs were performed as previously described (Pang et al., 2008). Soluble PA levels were determined by microplate assay using DMACA reagent, and the components of the soluble PAs analyzed using normal phase HPLC with postcolumn DMACA derivatization (Peel and Dixon, 2007). Levels of insoluble PAs in dried residues were determined by reaction with acid-butanol, and the butanol extracts were then separated by HPLC to determine the nature of the resulting anthocyanin units (Pang et al., 2008).

Phylogenetic and Topological Analysis

Alignment of protein sequences was done with ClustalW (http://www.ebi.ac.uk/clustalw/) using the default parameters. Formatting of aligned sequences was done with box shade program (http://www.ch.embnet.org/software/BOX_form.html). Sequence alignments were analyzed with Mesquite software, and the nonrooted neighbor-joining tree was generated by PAUP 4.0 BETA programs. All nodes are supported by at least 1000 bootstrap replicates. Topological analysis for transmembrane domains was performed using the TMHMM2 program in SMART (http://smart.embl-heidelberg.de).

Accession Numbers

Sequence data from this article can be found in the Arabidopsis Genome Initiative or GenBank/EMBL databases under the following accession numbers: *M. truncatula* MATE1, FJ858726; *Arabidopsis* TT12, NP_191462; *Vitis vinifera* AM1, FJ264202; *V. vinifera* AM3, FJ264203; *Zea mays* (maize) MTP77, AAQ55183; *Nicotiana tabacum* (tobacco) nicotine transporter, CAQ51477; *V. vinifera* predicted MATE transporters, XP_002282932 and CAO69962; *Populus trichocarpa* predicted MATE transporter, XP_002307572; *Brassica rapa* predicted MATE transporter, ACJ36213.

Supplemental Data

The following materials are available in the online version of this article.

Supplemental Figure 1. ATP-Dependent Flavonoid Glucoside Uptake into Vacuole-Enriched Vesicles from *M. truncatula* Hairy Roots Expressing *Arabidopsis* TT2.

Supplemental Figure 2. Competition of Uptake of E3′G, Cy3G, and D7G into Vacuole-Enriched Vesicles by Various Flavonoid Glucosides and Aglycones.

Supplemental Figure 3. Phylogenetic Analysis of Plant MATE Transporters.

Supplemental Figure 4. Amino Acid Alignments of *Arabidopsis* TT12 and *Medicago* MATE1.

Supplememtal Figure 5. Confocal Microscopy Image of MATE1-GFP Expressed in Yeast.

Supplemental Figure 6. Transport Properties of *Medicago* MATE1 Expressed in Yeast Cells.

Supplemental Figure 7. Subcellular Localization of MATE1-GFP Transiently Expressed in Tobacco Leaf Epidermal Cells, Viewed by Confocal Microscopy.

Supplemental Figure 8. PCR Analysis of PA Pathway Gene Transcripts in Wild-Type R108 and Seven Homozygous Progeny of *mate1*.

Supplemental Figure 9. Competition of the Uptake of Cy3G by E3′G in Yeast Microsomes Expressing *Arabidopsis* TT12.

Supplemental Figure 10. HPLC Chromatograph of Anthocyanins Released by Hydrolysis of Insoluble PAs in Butanol-HCl.

Supplemental Table 1. Primers Used in This Study.

Supplemental Data Set 1. Protein Sequences Used in Phylogenetic Analysis in Supplemental Figure 3.

Supplemental Data Set 2. Protein Sequences Used in Phylogenetic Analysis in Figure 3A.

ACKNOWLEDGMENTS

We thank Elison Blancaflor (Noble Foundation) for assistance with confocal microscopy, Parastoo Azadi (Complex Carbohydrate Research Center, University of Georgia at Athens) for NMR analysis, Markus Klein (University of Zurich) for provision of the *Arabidopsis TT12* cDNA, Isabelle Debeaujon (INRA, Versailles, France) for provision of seeds of the *Arabidopsis tt12* mutant, Carla Welch (Noble Foundation) for assistance with plant growth, Vagner Benedito (Noble Foundation) for help with qRT-PCR, and Vagner Benedito and Stephen Temple (Forage Genetics International) for critical reading of the manuscript. The *M. truncatula* plants used in this research project, which are jointly owned by the Centre National de la Recherche Scientifique, were created through research funded, in part, by Grant 703285 from the National Science Foundation. NMR analysis was supported in part by the Department of Energy-funded (DE-FG09-93R-20097) Center for Plant and Microbial Complex Carbohydrates. This work was supported by Forage Genetics International and the Samuel Roberts Noble Foundation.

Received April 9, 2009; revised July 8, 2009; accepted July 28, 2009; published August 14, 2009.

REFERENCES

Abrahams, S., Lee, E., Walker, A.R., Tanner, G.J., Larkin, P., and Ashton, A.R. (2003). The *Arabidopsis* TDS4 gene encodes leucoanthocyanidin dioxygenase (LDOX) and is essential for proanthocyanidin synthesis and vacuole development. Plant J. **35:** 624–636.

Abrahams, S., Tanner, G.J., Larkin, P.J., and Ashton, A.R. (2002). Identification and biochemical characterization of mutants in the

proanthocyanidin pathway in *Arabidopsis*. Plant Physiol. **130:** 561–576.

Ariga, T., Asao, Y., Sugimoto, H., and Yokotuska, T. (1981). Occurrence of astringent oligomeric proanthocyanidins in legume seeds. Agric. Biol. Chem. **45:** 2705–2708.

Bartholomew, D.M., Van Dyk, D.E., Lau, S.M., O'Keefe, D.P., Rea, P.A., and Viitanen, P.V. (2002). Alternate energy-dependent pathways for the vacuolar uptake of glucose and glutathione conjugates. Plant Physiol. **130:** 1562–1572.

Baxter, I.R., Young, J.C., Armstrong, G., Foster, N., Bogenschutz, N., Cordova, T., Peer, W.A., Hazen, S.P., Murphy, A.S., and Harper, J.F. (2005). A plasma membrane H^+-ATPase is required for the formation of proanthocyanidins in the seed coat endothelium of *Arabidopsis thaliana*. Proc. Natl. Acad. Sci. USA **102:** 2649–2654.

Benedito, V.A., et al. (2008). A gene expression atlas of the model legume *Medicago truncatula*. Plant J. **55:** 504–513.

Clough, S.J., and Bent, A.F. (1998). Floral dip: a simplified method for *Agrobacterium*-mediated transformation of *Arabidopsis thaliana*. Plant J. **16:** 735–743.

Debeaujon, I., Peeters, A.J.M., Leon-Kloosterziel, K.M., and Korneef, M. (2001). The *TRANSPARENT TESTA 12* gene of *Arabidopsis* encodes a multidrug secondary transporter-like protein required for flavonoid sequestration in vacuoles of the seed coat endothelium. Plant Cell **13:** 853–871.

Dixon, R.A., Xie, D.Y., and Sharma, S.B. (2005). Proanthocyanidins - A final frontier in flavonoid research? New Phytol. **165:** 9–28.

Drose, S., and Altendorf, K. (1997). Bafilomycins and concanamycins as inhibitors of V-ATPases and P-ATPases. J. Exp. Biol. **200:** 1–8.

Emans, N., Zimmermann, S., and Fischer, R. (2002). Uptake of a fluorescent marker in plant cells is sensitive to brefeldin A and wortmannin. Plant Cell **14:** 71–86.

Gabetta, B., Fuzzati, N., Griffini, A., Lolla, E., Pace, R., Ruffilli, T., and Peterlongo, F. (2000). Characterization of proanthocyanidins from grape seeds. Fitoterapia **71:** 162–175.

Gaxiola, R.A., Fink, G.R., and Hirschi, K.D. (2002). Genetic manipulation of vacuolar proton pumps and transporters. Plant Physiol. **129:** 967–973.

Gomez, C., Terrier, N., Torregrosa, L., Vialet, S., Fournier-Level, A., Verries, C., Souquet, J.M., Mazauric, J.P., Klein, M., Cheynier, V., and Ageorges, A. (2009). Grapevine MATE-type proteins act as vacuolar H+-dependent acylated anthocyanin transporters. Plant Physiol. **150:** 402–415.

Goodman, C.D., Casati, P., and Walbot, V. (2004). A multidrug resistance-associated protein involved in anthocyanin transport in *Zea mays*. Plant Cell **16:** 1812–1826.

Grotewold, E. (2004). The challenges of moving chemicals within and out of cells: Insights into the transport of plant natural products. Planta **219:** 906–909.

Gu, L., Kelm, M.A., Hammerstone, J.F., Beecher, G., Holden, J., Haytowitz, D., Gebhardt, S., and Prior, R.L. (2004). Concentrations of proanthocyanidins in common foods and estimations of normal consumption. J. Nutr. **134:** 613–617.

He, F., Pan, Q.-H., Shi, Y., and Duan, C.-Q. (2008). Biosynthesis and genetic regualtion of proanthocyanidins in plants. Molecules **13:** 2674–2703.

Hunter, P.R., Craddock, C.P., Di Benedetto, S., Roberts, L.M., and Frigerio, L. (2007). Fluorescent reporter proteins for the tonoplast and the vacuolar lumen identify a single vacuolar compartment in Arabidopsis cells. Plant Physiol. **145:** 1371–1382.

Kitamura, S. (2006). Transport of flavonoids. From cytosolic synthesis to vacuolar accumulation. In The Science of Flavonoids, E. Grotewald, ed (New York: Springer), pp. 123–146.

Kitamura, S., Shikazono, N., and Tanaka, A. (2004). TRANSPARENT TESTA 19 is involved in the accumulation of both anthocyanins and proanthocyanidins in *Arabidopsis*. Plant J. **37:** 104–114.

Klein, M., Weissenbock, G., Dufaud, A., Gaillard, C., Kreuz, K., and Martinoia, E. (1996). Different energization mechanisms drive the vacuolar uptake of a flavonoid glucoside and a herbicide glucoside. J. Biol. Chem. **271:** 29666–29671.

Koupai-Abyazani, M.R., McCallum, J., Muir, A.D., Lees, G.L., Bohm, B.A., Towers, G.H.N., and Gruber, M.Y. (1993). Purification and characterization of a proanthocyanidin polymer from seed of alfalfa (*Medicago sativa* cv. beaver). J. Agric. Food Chem. **41:** 565–569.

Lee, Y., Yoon, H.R., Paik, Y.S., Liu, J.R., Chung, W.I., and Choi, G. (2005). Reciprocal regulation of Arabidopsis UGT78D2 and BANYULS is critical for regulation of the metabolic flux of anthocyanidins to condensed tannins in developing seed coats. J. Plant Biol. **48:** 356–370.

Lees, G.L. (1992). Condensed tannins in some forage legumes: Their role in the prevention of ruminant pasture bloat. Basic Life Sci. **59:** 915–934.

Lefebvre, B., Batoko, H., Duby, G., and Boutry, M. (2004). Targeting of a *Nicotiana plumbaginifolia* H^+-ATPase to the plasma membrane is not by default and requires cytosolic structural determinants. Plant Cell **16:** 1772–1789.

Lepiniec, L., Debeaujon, I., Routaboul, J.-M., Baudry, A., Pourcel, L., Nesi, N., and Caboche, M. (2006). Genetics and biochemistry of seed flavonoids. Annu. Rev. Plant Biol. **57:** 405–430.

Li, Y.G., Tanner, G., and Larkin, P. (1996). The DMACA-HCl protocol and the threshold proanthocyanidin content for bloat safety in forage legumes. J. Sci. Food Agric. **70:** 89–101.

Luvisetto, S., and Azzone, G.F. (1989). Local protons and uncoupling of aerobic and artificial delta muH-driven ATP synthesis. Biochemistry **28:** 1109–1116.

Marinova, K., Pourcel, L., Weder, B., Schwarz, M., Barron, D., Routaboul, J.-M., Debeaujon, I., and Klein, M. (2007). The *Arabidopsis* MATE transporter TT12 acts as a vacuolar flavonoid/H+-antiporter active in proanthocyanidin-accumulating cells of the seed coat. Plant Cell **19:** 2023–2038.

Marles, M.A.S., Ray, H., and Gruber, M.Y. (2003). New perspectives on proanthocyanidin biochemistry and molecular regulation. Phytochemistry **64:** 357–383.

Morita, M., Shitan, N., Sawada, K., Van Montagu, M.C., Inzé, D., Rischer, H., Goossens, A., Oksman-Caldentey, K.M., Moriyama, Y., and Yazaki, K. (2009). Vacuolar transport of nicotine is mediated by a multidrug and toxic compound extrusion (MATE) transporter in *Nicotiana tabacum*. Proc. Natl. Acad. Sci. USA **106:** 2447–2452.

Naoumkina, M., Farag, M.A., Sumner, L.W., Tang, Y., Liu, C.-J., and Dixon, R.A. (2007). Different mechanisms for phytoalexin induction by pathogen and wound signals in *Medicago truncatula*. Proc. Natl. Acad. Sci. USA **104:** 17909–17915.

Nakanishi, Y., Saijo, T., Wada, Y., and Maeshima, M. (2001). Mutagenic analysis of functional residues in putative substrate-binding site and acidic domains of vacuolar H^+-pyrophosphatase. J. Biol. Chem. **276:** 7654–7660.

Pang, Y., Peel, G.J., Sharma, S.B., Tang, Y., and Dixon, R.A. (2008). A transcript profiling approach reveals an epicatechin-specific glucosyltransferase expressed in the seed coat of *Medicago truncatula*. Proc. Natl. Acad. Sci. USA **105:** 14210–14215.

Pang, Y., Peel, G.J., Wright, E., Wang, Z., and Dixon, R.A. (2007). Early steps in proanthocyanidin biosynthesis in the model legume *Medicago truncatula*. Plant Physiol. **145:** 601–615.

Peel, G.J., and Dixon, R.A. (2007). Detection and quantification of engineered proanthocyanidins in transgenic plants. Nat. Prod. Commun. **2:** 1009–1014.

Peel, G.J., Modolo, L.V., Pang, Y., and Dixon, R.A. (2009). The LAP1

MYB transcription factor orchestrates anthocyanidin biosynthesis and glycosylation in Medicago. Plant J. **59:** 136–149.

Pezza, R.J., Villarreal, M.A., Montich, G.G., and Argaraña, C.E. (2002). Vanadate inhibits the ATPase activity and DNA binding capability of bacterial MutS. A structural model for the vanadate-MutS interaction at the Walker A motif. Nucleic Acids Res. **30:** 4700–4708.

Pfaffl, M.W. (2001). A new mathematical model for relative quantification in real-time RT-PCR. Nucleic Acids Res. **29:** e45.

Poustka, F., Irani, N.G., Feller, A., Lu, Y., Pourcel, L., Frame, K., and Grotewald, E. (2007). A trafficking pathway for anthocyanins overlaps with the endoplasmic reticulum-to-vacuole protein-sorting route in Arabidopsis and contributes to the formation of vacuolar inclusions. Plant Physiol. **145:** 1323–1335.

Ramakers, C., Ruijter, J.M., Deprez, R.H., and Moorman, A.F. (2003). Assumption-free analysis of quantitative real-time polymerase chain reaction (PCR) data. Neurosci. Lett. **13:** 62–66.

Rodrigues, C.O., Scott, D.A., and Docampo, R. (1999). Presence of a vacuolar H+ pyrophosphatase in promastigotes of *Leishmania donovani* and its localization to a different compartment from the vacuolar H+-ATPase. Biochem. J. **340:** 759–766.

Routaboul, J.-M., Kerhoas, L., Debeaujon, I., Pourcel, L., Caboche, M., Einhorn, J., and Lepiniec, L. (2006). Flavonoid diversity and biosynthesis in seed of *Arabidopsis thaliana*. Planta **224:** 96–107.

Santos-Buelga, C., and Scalbert, A. (2000). Proanthocyanidins and tannin-like compounds-nature, occurrence, dietary intake and effects on nutrition and health. J. Sci. Food Agric. **80:** 1094–1117.

Serafini, M., Bugianesi, R., Maiani, G., Valtuena, S., De Santis, S., and Crozier, A. (2003). Plasma antioxidants from chocolate. Nature **424:** 1013.

Shimoda, K., Otsuka, T., Morimoto, Y., Hanada, H., and Hanada, H. (2007). Glycosylation and malonylation of quercetin, epicatechin, and catechin by cultured plant cells. Chem. Lett. **36:** 1292–1293.

Shirley, B.W., Kubasek, W.L., Storz, G., Bruggemann, E., Koornneef, M., Ausubel, F.M., and Goodman, H.M. (1995). Analysis of Arabidopsis mutants deficient in flavonoid biosynthesis. Plant J. **8:** 659–671.

Shoji, T., Inai, K., Yazaki, Y., Sato, Y., Takase, H., Shitan, N., Yazaki, K., Goto, Y., Toyooka, K., Matsuoka, K., and Hashimoto, T. (2009). Multidrug and toxic compound extrusion-type transporters implicated in vacuolar sequestration of nicotine in tobacco roots. Plant Physiol. **149:** 708–718.

Sugiyama, A., Shitan, N., and Yazaki, K. (2007). Involvement of a soybean ATP-binding cassette-type transporter in the secretion of genistein, a signal flavonoid in legume-*Rhizobium* symbiosis. Plant Physiol. **144:** 2000–2008.

Sutter, J.U., Campanoni, P., Tyrrell, M., and Blatt, M.R. (2006). Selective mobility and sensitivity to SNAREs is exhibited by the *Arabidopsis* KAT1 K^+ channel at the plasma membrane. Plant Cell **18:** 935–954.

Tadege, M., Wen, J., He, J., Tu, H., Kwak, Y., Eschstruth, A., Cayrel, A., Endre, G., Zhao, P.X., Chabaud, M., Ratet, P., and Mysore, K.S. (2008). Large scale insertional mutagenesis using Tnt1 retrotransposon in the model legume *Medicago truncatula*. Plant J. **54:** 335–347.

Terrier, N., Torregrosa, L., Ageorges, A., Vialet, S., Verriès, C., Cheynier, V., and Romieu, C. (2009). Ectopic expression of VvMybPA2 promotes proanthocyanidin biosynthesis in grapevine and suggests additional targets in the pathway. Plant Physiol. **149:** 1028–1041.

Verweij, W., Spelt, C., Di Sansebastiano, G.-P., Vermeer, J., Reale, L., Ferranti, F., Koes, R., and Quattrocchio, F. (2008). An H^+ P-ATPase on the tonoplast determines vacuolar pH and flower colour. Nat. Cell Biol. **10:** 1456–1462.

Xie, D.-Y., and Dixon, R.A. (2005). Proanthocyanidin biosynthesis- still more questions than answers? Phytochemistry **66:** 2126–2143.

Xie, D.Y., Sharma, S.B., Paiva, N.L., Ferreira, D., and Dixon, R.A. (2003). Role of anthocyanidin reductase, encoded by *BANYULS* in plant flavonoid biosynthesis. Science **299:** 396–399.

Yazaki, K. (2005). Transporters of secondary metabolites. Curr. Opin. Plant Biol. **8:** 301–307.

Zhao, J., Shigaki, T., Mei, H., Guo, Y.Q., Cheng, N.H., and Hirschi, K.D. (2009). Interaction between Arabidopsis Ca^{2+}/H^+ exchangers CAX1 and CAX3. J. Biol. Chem. **284:** 4605–4615.